Geomorphology 483 (2025) 109796

Contents lists available at ScienceDirect

Geomorphology

journal homepage: www.journals.elsevier.com/geomorphology

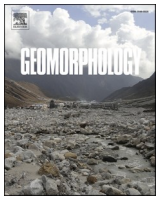

Relative sea-level changes and reef development in the northern Coral Triangle during the late Quaternary

Kathrine Maxwell [a,b,c,*], Alessio Rovere [d,e], Hildegard Westphal [a,b], Kevin Garas [f], Mirasol Guinto [g], Denovan Chauveau [d,h], Hsun-Ming Hu [i,j], Chuan-Chou Shen [i,j]

[a] Leibniz Centre for Tropical Marine Research (ZMT), Bremen, Germany
[b] University of Bremen, Department of Geosciences, Bremen, Germany
[c] Senckenberg am Meer Wilhelmshaven, Marine Research Department, Wilhelmshaven, Germany
[d] Department of Environmental Sciences, Informatics and Statistics, Ca' Foscari University of Venice, Venice, Italy
[e] MARUM - Center for Marine Environmental Sciences, University of Bremen, Bremen, Germany
[f] Department of Environment and Natural Resources–Mines and Geosciences Bureau (DENR-MGB), Quezon City 1100, Philippines
[g] Forestry Development Center, College of Forestry and Natural Resources, University of the Philippines, Los Baños, Laguna, Philippines
[h] Geo-Ocean, UMR 6538, CNRS, Ifremer, Université de Bretagne Occidentale, F-29280 Plouzané, France
[i] High-Precision Mass Spectrometry and Environment Change Laboratory (HISPEC), Department of Geosciences, National Taiwan University, Taipei, 10617, Taiwan, ROC
[j] Research Center for Future Earth, National Taiwan University, Taipei 10617, Taiwan, ROC

ARTICLE INFO

Keywords:
Relative sea-level change
Coral Triangle
Coral reef terraces
Late Quaternary

ABSTRACT

The Philippines, situated at the apex of the Coral Triangle, is fringed by both modern and fossil coral reefs that preserve valuable records of Quaternary relative sea-level changes and tectonic deformation. This study presents a new interpretation of the formation of the Late Pleistocene coral reef terraces at Cape Bolinao in western Luzon, offering insights into sea-level history, reef development, and tectonic uplift within the northern Coral Triangle. Integrating high-resolution morphological analysis, new geochronological data, and reef stratigraphic numerical models, we delineate nine distinct reef terraces. The lowest terrace (~4 m above mean sea level) dates to the mid-Holocene, while reef simulations replicating present-day terrace morphology constrain the highest terrace (~155 m amsl) to Marine Isotope Stage (MIS) 5e, indicating a long-term uplift rate of 1.17 ± 0.03 mm/yr for Cape Bolinao. We propose a morpho-chronologic framework wherein a Late Pleistocene table reef developed on a gently sloping substrate and was progressively uplifted, leading to successive fringing reef terraces. This high uplift, coupled with observed tilting and deformation patterns, provides compelling evidence that subduction of the Scarborough Seamount Chain beneath Luzon Island exerts a primary control on localized forearc deformation along the Manila Subduction Zone. This work offers a key dataset for understanding Quaternary CRT development in the northern Coral Triangle and sheds light on how subduction-related processes have shaped the region's sea-level and coral reef records.

1. Introduction

Coral reef terraces (CRTs) are formed through repeated bio-constructional and erosional processes, and they can be used as indicators of relative sea-level changes through time (e.g., Anthony, 2008; Rovere et al., 2016). The occurrence and exposure of late Quaternary CRTs above present sea level are proxies of past relative sea-level changes as their formation, growth, and geomorphological development are primarily controlled by changes in eustatic sea level and/or vertical land motions (e.g., Woodroffe and Webster, 2023). The analysis of sea-level indicators during previous interglacials allows insights into potential drivers of relative sea-level changes in the past (e.g., Rovere et al., 2016). In areas considered tectonically stable (Yucatan peninsula, Mexico, e.g., Blanchon et al., 2009) or active (Huon Peninsula, e.g., De Gelder et al., 2022), exposed fossil coral reef terraces provide accessible record of relative sea-level change, such as during the Last Interglacial (Marine Isotope Stage (MIS) 5e, ~130–116 ka) when eustatic sea level was higher than present, by 2 to 9 m (e.g., Dutton and Lambeck, 2012;

* Corresponding author at: Leibniz Centre for Tropical Marine Research (ZMT), Bremen, Germany.
E-mail address: kathrine.maxwell@senckenberg.de (K. Maxwell).

https://doi.org/10.1016/j.geomorph.2025.109796
Received 1 July 2024; Received in revised form 15 April 2025; Accepted 21 April 2025
Available online 24 April 2025

Dyer et al., 2021; Dumitru et al., 2023). Meanwhile, in subsiding regions (e.g., Tahiti), sea-level reconstructions are based on sedimentological and paleontological data from offshore drill cores allowing the investigation of relict reef features related to glacial-interglacial periods (e.g., Camoin et al., 2012; Deschamps et al., 2012).

In tectonically active regions, exposed sequences of fossil CRT document a combined signal of eustatic sea-level and tectonic uplift (e.g., Chappell, 1974; Lajoie, 1986; Pedoja et al., 2011, 2018; Maxwell et al., 2021; Peñalver et al., 2021). In the Ryukyu Islands in southwestern Japan, CRTs in Kikai Island yielded MIS 5e uplift rates from 1.8 to 2.2 mm/yr which reflect active deformation on the leading edge of an overriding Eurasian Plate (e.g., Ota and Omura, 1992; Inagaki and Omura, 2006). Previous works on the canonical CRTs of Huon Peninsula (Papua New Guinea), situated along the boundary between the Australian and West Pacific plates, identified uplift rates as high as 3.3 to 3.5 mm/yr (e.g., Chappell, 1974; Chappell et al., 1996a). Corrected for

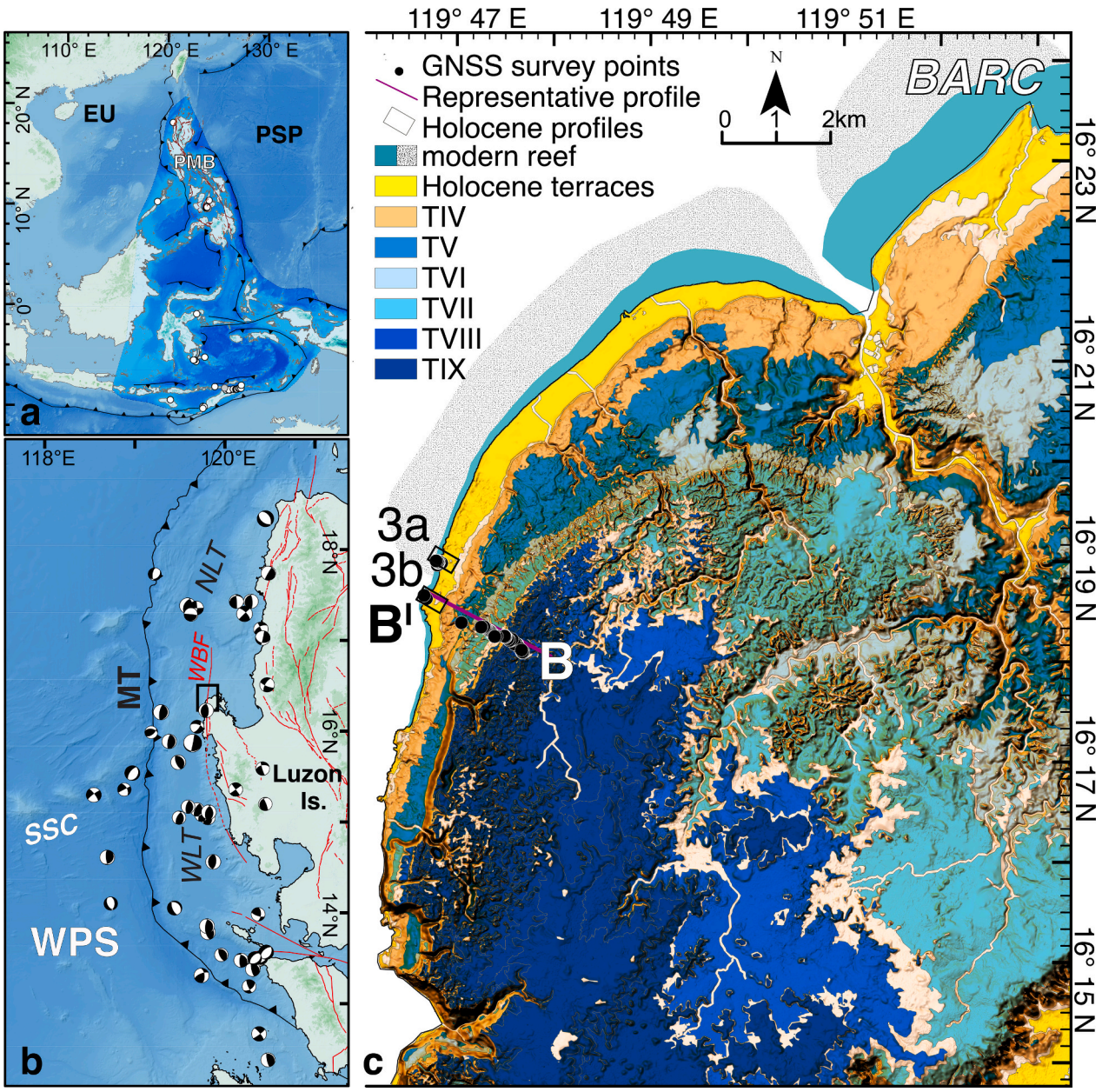

Fig. 1. Cape Bolinao and its location along the western Philippines at the apex of the Coral Triangle. **a.** Map of Southeast Asia and the Coral Triangle (shaded in blue). Circles show the previously reported Last Interglacial (LIG) CRTs in the region as compiled in Maxwell et al. (2021). **b.** Tectonic elements bordering western Luzon Island and location of Cape Bolinao (in black box). Focal mechanism solutions (>M5) were obtained from the Global CMT Project (Dziewonski et al., 1981; Ekström et al., 2012) and in red lines, the active faults traversing the PMB from the PHIVOLCS (2020). **c.** Surface classification model (SCM) showing the different paleo-reef surfaces in Cape Bolinao. The highest terrace (TIX, in dark blue) indicates the oldest fossil coral reef terrace mapped and the lowest terrace (in yellow) are the Holocene reefs. Also shown is the location of the present-day reef, the Bolinao-Anda Reef Complex (BARC), from McManus et al. (1992). The survey sites in Patar, Bolinao: (1) Rockview Point (in Fig. 3a) and (2) Punta Piedra Point (in Fig. 3b) are bounded by boxes. The representative profile, B–B^{I}, (Fig. 7) is also shown. Basemaps were created using topography data from Japan Aerospace Exploration Agency (JAXA) ALOS World 3D–30 m (AW3D30) (https://www.eorc.jaxa.jp/ALOS/en/dataset/aw3d30/aw3d30_e.htm) and bathymetry data from the GEBCO Compilation Group (2023) GEBCO 2023 Grid (doi:https://doi.org/10.5285/f98b053b-0cbc-6c23-e053-6c86abc0af7b). Maps were created using ESRI ArcGIS Pro 3.1 and the Generic Mapping Tools (GMT) software (Wessel et al., 2019). PSP: Philippine Sea Plate; EU: Eurasian Plate; MT: Manila Trench; WLT: West Luzon Trough; WPS: West Philippine Sea; NLT: North Luzon Trough; WBF: Western Boundary Fault; SSC: Scarborough Seamount Chain.

tectonics and post-depositional land movements, uplifted CRTs offer a detailed record of relative sea-level change since MIS 5e and has been converted into estimates of ice volume changes over the last climatic cycle (e.g., Chappell, 1974; Bloom et al., 1974; Chappell et al., 1996b; Lambeck and Chappell, 2001; Yokoyama and Esat, 2011). The CRTs in Barbados (e.g., Mesolella, 1967; Broecker et al., 1968; Blanchon and Eisenhauer, 2001; Schellmann and Radtke, 2004) and in Sumba Island in Indonesia (e.g., Pirazzoli et al., 1991, 1993; Bard et al., 1996) present a relative sea-level record spanning the last 1 Ma where Late and Middle Pleistocene terraces are dated.

Numerical models of reef growth allow modelling the processes that contribute to the creation of CRTs, accounting for changes in sea level, vertical land motion, reef growth rate, wave erosion, and initial substrate slope (e.g., Koelling et al., 2009; Husson et al., 2018; Pastier et al., 2019; De Gelder et al., 2020). These landscape evolution models help understand the geomorphic responses of coral reef sequences to changes in sea level and provide additional constraints on the potential timing and development of the reef sequences, especially when CRT ages are poorly constrained (e.g., Chauveau et al., 2023, 2024; Boyden et al., 2023; De Gelder et al., 2023). For example, in Huon Peninsula, the analysis of high-resolution digital elevation models coupled with numerical models of coral reef terrace formation allowed elucidating the morphogenesis of reef terraces over the last 420 kyr and further suggest that oxygen isotope-based global mean sea-level curves systematically underestimate interstadial sea-level elevations, by up to ~20 m (De Gelder et al., 2022). In Sumba Island, numerical reef modelling shows that at least two terraces can be created during MIS 5e and multiple sea-level peaks during MIS 5e are not required to explain the presence of these terraces (Chauveau et al., 2023).

In the Philippines, there is little information available about the geomorphological evolution of the emergent CRTs in Cape Bolinao, west Luzon, northern Coral Triangle (see previous works of Maemoku and Paladio, 1992 and Ramos and Tsutsumi, 2010). We aim to fill this gap by exploring the morphological development of the Cape Bolinao CRTs using high-resolution digital elevation models and numerical models based on new geomorphic, geochronologic, and morpho-stratigraphic data. While no comprehensive chronological framework has been proposed for Cape Bolinao so far, we couple our geomorphic analysis with numerical reef modelling to help constrain the chronology, as well as investigate uplift and CRT morphogenesis.

2. Regional geology and tectonic setting

Cape Bolinao (Fig. 1) is located in the western portion of Luzon Island, Philippines, at the northern apex of the Coral Triangle, which is a region known as the epicenter of marine biodiversity (e.g., Hoeksema, 2007; Veron et al., 2009; Veron et al., 2015). From a tectonic standpoint, Cape Bolinao lies at the western portion of the Philippine Mobile Belt (PMB), a 400-km wide deformation zone from Luzon to Mindanao, Philippines, which resulted from the WNW oblique convergence of the Philippine Sea Plate (PSP) and the Eurasian Plate (EU) (e.g., Gervasio, 1967; Rangin et al., 1999). It faces the West Philippine Sea and is bounded to the west by the Manila Trench (MT) subduction zone, an active convergent plate margin, along which, the South China Sea oceanic basin is being subducted eastward (e.g., Hayes and Lewis, 1985). Recent estimates based on GPS data reveal a convergence rate of 91 mm/yr at the northern end of Luzon and 55 mm/yr in the south and a highly coupled (relatively locked) region between the West Luzon Trough (WLT) and the east of the Scarborough Seamount Chain (SSC) (Hsu et al., 2012).

Cape Bolinao is predominantly underlain by the Plio-Pleistocene coralline reefal limestone named the Bolinao Limestone (Mines and Geosciences Bureau, 2010; Supplementary Fig. 1a). Lithologic units underlying the Bolinao Limestone are interbedded sandstone, siltstone, and claystone which were assigned Late Pliocene (Piacenzian) based on holoplanktonic gastropods (Janssen, 2007) to Early Pleistocene (1.77 to 0.61 Ma) based on nannofossils and planktonic foraminifers (Wani et al., 2008). These lithologic units were interpreted to indicate an epi- to upper meso-pelagic setting, with depth ranges extending to a maximum of 200–300 m water depth (Janssen, 2007). Underlying the Bolinao Limestone is the Late Miocene to Early Pliocene Santa Cruz Formation (Mines and Geosciences Bureau, 2010). Along the western coast of Cape Bolinao, a sequence of CRTs rising to about ~155 m above mean sea level (amsl) is observed (Fig. 2). This was first described by Maemoku and Paladio (1992) who identified seven terraces from interpretation of aerial photos and altimeter measurements. Their classification was based on elevation and degree of dissection, and they assumed that the highest terrace was MIS 5e in age and the lowest one was Holocene.

The extensive modern fringing reef (Fig. 1c) along the northeastern portion of Cape Bolinao is referred to as the Bolinao-Anda Reef Complex (BARC). This reef has an area of ~200 km^2, and it is composed of three distinct zones: a reef flat and lagoon, an intertidal reef crest, and a fore reef (Fig. 2a, McManus et al., 1992; Vergara et al., 2010). The reef flat and lagoon are primarily dominated by seagrass with occasional patches of living and dead corals, as well as sandy-muddy substrates. Depths in this zone range from 0.3 to 6 m, with an average of 2 m (e.g., Shaish et al., 2010; Cantarero et al., 2019) and the substrate is mostly rocky to sandy, often covered with seagrasses, seaweeds, coral boulders, and occasional living coral heads (e.g., microatolls) (Fig. 2b–d). The intertidal reef crest features dead coral rubble interspersed with patches of live coral colonies, while the fore reef is characterized by gentle to steep slopes of variable depths (10–30 m) and a talus of sand and coral rubble extending ~22 km into the middle of the Lingayen Gulf (Fig. 2, McManus et al., 1992; Vergara et al., 2010).

Coral communities and benthic composition across the BARC exhibit substantial spatial variability (e.g., Quimpo et al., 2020). Branching and massive corals from families such as Acroporidae, Pocilloporidae, Poritidae, and Helioporidae are particularly abundant (e.g., Shaish et al., 2010; Torres et al., 2021). For instance, Caniogan Reef in southeastern BARC is dominated by hard corals like *Astreopora*, *Acropora*, and *Pocillopora*, alongside sand and coral rubble (Quimpo et al., 2020). In contrast, Balingasay Reef on the western side is characterized by massive corals such as *Dipsastrea* and *Porites*, as well as *Heliopora* (Quimpo et al., 2020). Other benthic components commonly observed across the reef include turf algae, macroalgae, crustose coralline algae, soft corals, gorgonians, zoanthids, and a variety of invertebrates such as anemones, ascidians, bryozoans, mollusks, clams, and sea urchins (e.g., Quimpo et al., 2020). Dead coral fragments, sand, and rubble also contribute significantly to the benthic environment. Despite these observations, no comprehensive study has systematically documented the distribution of coral morphologies and species across the full extent of BARC's modern reef profile. Existing literature provides only a general overview of its ecological characteristics. A detailed modern reef survey remains beyond the scope of this study.

In our survey sites (that are usually exposed to high-energy wave conditions), the modern reef flat is limited towards the sea by the reef edge, which is in turn characterized by spurs and grooves, with its landward edge marked by discontinuous rocky cliffs and stretches of sandy beaches (Fig. 2b). Etched onto rocky cliffs are shoreline angles and sometimes, tidal notches (Fig. 2a). Shoreline angles (sometimes referred to as inner margins, e.g., Maxwell et al., 2018) are located at the intersection between the reef platform and the sea cliff and are used as a morphological approximation of paleo-shorelines (e.g., Lajoie, 1986). Tides in this area are mainly semidiurnal, with a mean tidal range of 0.65 m according to data from the nearest primary station of the Department of Environment and Natural Resources-National Mapping and Resource Information Authority (DENR-NAMRIA) in San Fernando, La Union.

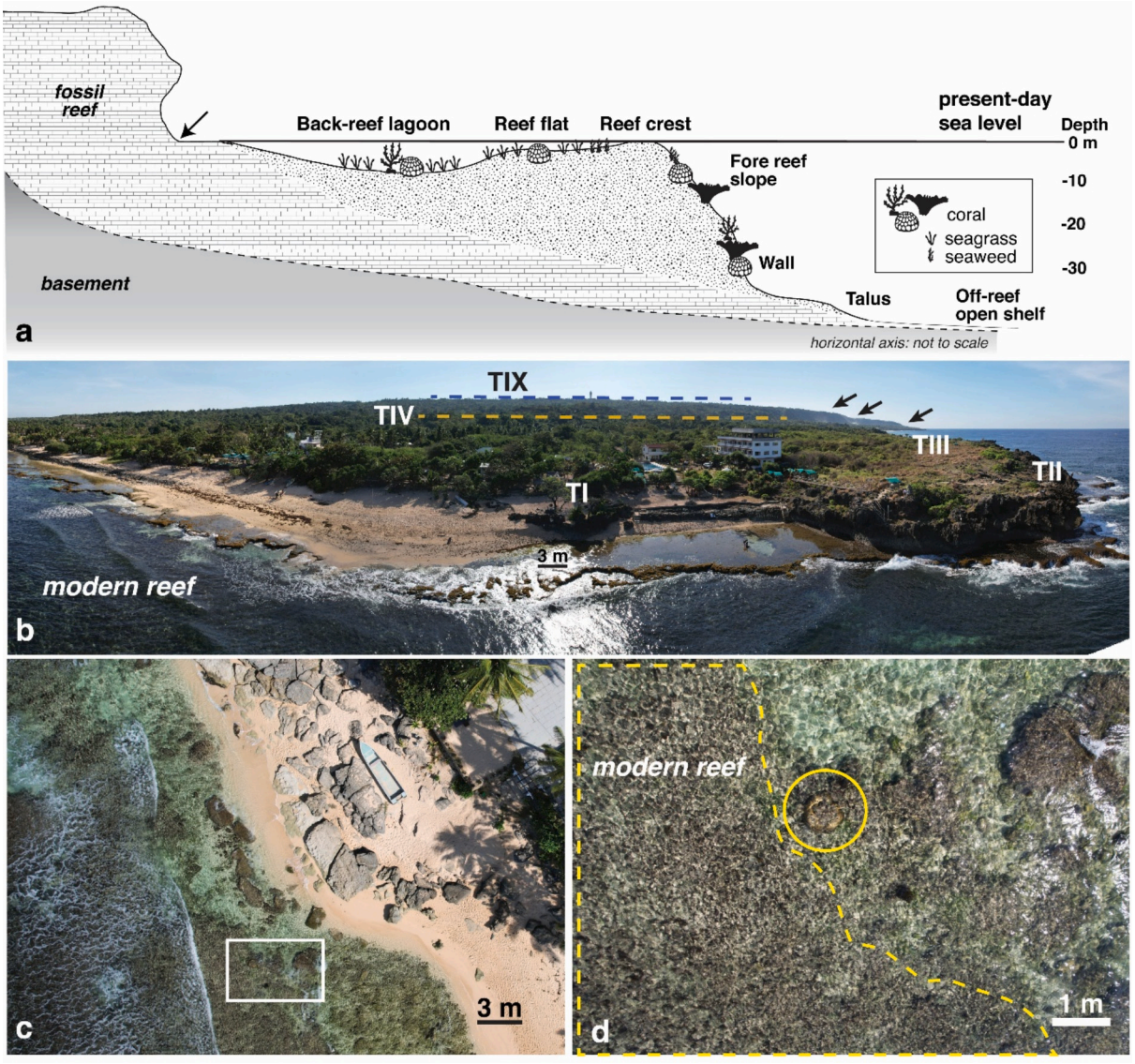

Fig. 2. Coral reef terraces in Cape Bolinao. **a.** Schematic diagram of the BARC and the relationship of shoreline angle (black arrow) with present-day sea level. The modern-day reef profile, dominated by seagrass and occasional patches of living and dead corals, is based on the descriptions of McManus et al. (1992) and Vergara et al. (2010). The figure is not to scale for illustrative purposes. **b.** Aerial photo (view looking SE) of the CRTs as observed in Punta Piedra Point. Lower terraces (TI-TIII) are recognized at elevations <9 m and higher terraces are highlighted by dashed lines (TIV and TIX) and black arrows. **c–d.** Aerial photos of the modern reef flat characterized by a dominance of seagrass with occasional patches of living corals and dead coral boulders. White box shows the location of photo (d), which shows a living coral (i.e., microatoll, bounded by yellow circle) surrounded by seagrass (bounded by yellow dashed line).

3. Methods

3.1. Coral reef terrace mapping

Fossil CRTs were mapped on digital elevation models (DEMs), satellite images, and topographic surveys. We used the 2013 airborne Interferometric Synthetic Aperture Radar-derived-Digital Terrain Model (IFSAR-DTM) with 5-meter posting provided by the National Mapping and Resource Information Authority (NAMRIA) to generate derivative maps (e.g., hillshade, contour, slope, aspect), which allowed us to examine the morphology of the CRT sequences in Cape Bolinao. Using the TerraceM-2 program (Jara-Muñoz et al., 2019) and topographic slope and roughness, we generated a surface classification model (SCM) to delineate semi-automatically paleo-reef platforms and steeper areas that may represent paleo-cliffs.

Systematic topographic surveys, orthogonal to the modern shoreline, were carried out along accessible portions of the coast. We took a particular interest at the section where all the terraces were well preserved and previously described (Maemoku and Paladio, 1992; Ramos and Tsutsumi, 2010). To measure the location and elevation of points of interest, we used a pair of Emlid REACH RS+ single-band Global Navigation Satellite systems (GNSS) receivers with a Base-Rover configuration and connected with the nearest PURD station of the Philippine Active Geodetic Network (PAGeNet)-NAMRIA. Elevation data was referred to orthometric heights using the Philippine Geoid Model 2018 (PGM2018) of NAMRIA (Gatchalian et al., 2021). We discarded data points with elevation RMS values higher than ±1 m and retained the data point with the lowest elevation RMS whenever several measurements were taken for the same point. Sources of vertical error include the elevation RMS per data point and the estimated accuracy of the PGM2018 model of ±0.012 m. Taking these into account, the elevation error of our GNSS data range from ±0.011 to ±0.123 m. To supplement and fill the gaps in our survey data (especially in areas where network coverage is poor), we also extracted topographic profiles, orthogonal to

the coast, from the IFSAR-DTM (<1-meter vertical accuracy). Heights of paleo reefs, shoreline angles, and fossil coral samples are reported in meters above mean sea level (m amsl). Data processing and map generation were done using the ArcGIS Pro software by Environmental Systems Research Institute (ESRI).

3.2. Reef terrace composition and geochronology

Select exposed outcrops of CRTs were examined, and rock samples were collected and petrographically described. Fossil corals and mollusks found *in situ* in original growth or life position were collected for radiometric dating. Corals, primarily of the genera *Porites*, *Goniastrea*, and *Acropora*, were sampled from exposed reef terrace platform surfaces. Classification of *in situ* samples was based on a combination of morphological and stratigraphic criteria commonly used in reef terrace studies. Corals were considered *in situ* if they exhibited upright growth orientation with intact basal attachment, were embedded within consolidated reef framework, and showed no evidence of reworking, such as overturned bedding, loose clasts, or disarticulated fragments. Mollusks were similarly classified as *in situ* if they were found articulated, preserved in life position, or enclosed within undisturbed reef deposits. Priority was given to well-preserved specimens, and any signs of reworking or disturbance were explicitly recorded. Visual screening for calcite recrystallization was done in the field, and samples were extracted by chipping from the outer rims of coral colonies with diameters of at least 20 cm. Elevations of samples were measured and reported in m amsl.

Additional screening for samples includes preparing thin sections and visually examining them under the microscope to assess the presence of diagenetic textures. Our assessment followed the visual criteria and classification guidelines of McGregor and Abram (2008), which provided a standardized framework for evaluating coral preservation. Based on this approach, we petrographically classified the coral samples as either having "excellent" preservation with no diagenetic textures observed equivalent to calcite below detection levels or having "good" preservation with rare diagenetic textures observed. Samples outside these categories were discarded. Coral samples exhibiting well-preserved aragonitic skeletal elements with minimal evidence of secondary aragonite, calcite, or other diagenetic features (i.e., those falling into the "good" category) were selected for radiocarbon and U-Th dating (Supplementary Fig. 2a–b). During this screening process, all coral samples from Terraces II to IX were rejected due to clear signs of calcite recrystallization and diagenetic alteration, as identified through visual and petrographic analysis (Supplementary Fig. 2c–h). Given the extent of diagenetic alteration, further testing using X-ray diffraction (XRD) was deemed unnecessary. Only coral samples from Terrace I, which showed very little evidence of such alteration, were considered suitable for geochronological analysis.

After screening, we sent eight coral subsamples to the High-Precision Mass Spectrometry and Environment Change Laboratory (HISPEC) at the National Taiwan University to be analyzed for U-Th isotopic compositions using a high-resolution multi-collector inductively coupled plasma mass spectrometer (MC-ICP-MS), Thermo Fisher Neptune. Chemistry followed the procedure described in Shen et al. (2003) and instrumental analysis used the protocols given in Shen et al. (2013). Analytical errors are reported at the two-sigma (2s) of the mean. ^{230}Th ages with 2-sigma uncertainty ranges are reported in years before present (year BP) relative to 1950 CE. Radiocarbon dating of three coral subsamples and two *Tridacna* subsamples was conducted in the Beta Analytic Radiocarbon Dating Laboratory in Miami, Florida, U.S.A by Accelerator Mass Spectrometry (AMS) method. The OxCal version 4.4 (Bronk Ramsey, 2009) was used to calibrate conventional radiocarbon ages using the MARINE20 Marine Radiocarbon Age Calibration Curve (Heaton et al., 2020). We calculated the local DeltaR correction of -262 ± 63 for Cape Bolinao based on coupled ^{14}C and ^{230}Th ages of three coral samples using an online application for DeltaR calculation (Reimer and Reimer, 2017). Radiocarbon ages presented in this study are reported in calibrated years before present (cal BP) relative to 1950 CE. Given the good preservation of the dated samples, initial $^{234}U/^{238}U$ activity ratios ($\delta^{234}U_{initial}$ values) within acceptable limits, and the strong agreement between the ^{230}Th and ^{14}C ages, we consider the ages reported in this study to be reliable.

3.3. Terrace morphology and deformation

To systematically visualize the lateral and vertical extent of the emergent CRTs in Cape Bolinao, we employed large-scale parallel swath profiles, which were stacked to create composite swath profiles (e.g., Armijo et al., 2015; Fernández-Blanco et al., 2020; De Gelder et al., 2022). These stacked swath profiles, which appear as clusters of overprinted elevation profiles, highlight topographic coherence along the viewing direction and the consistency of slope and morphology perpendicular to it (De Gelder et al., 2022; Chauveau et al., 2023).

We generated the stacked swath profiles using the TopoToolbox 2, a MATLAB-based software for topographic analysis by Schwanghart and Scherler (2014). To achieve this, we created swaths, from sets of 100–300 parallel lines. The swath width, set at either 50 m or 100 m, was carefully selected to balance data resolution and noise reduction while ensuring full spatial coverage of the study area. The swaths, aligned parallel to their length, represent the cross-sectional area where topographic data are averaged to derive elevation profiles, minimizing biases associated with discrete topographic profiles (e.g., Armijo et al., 2015; Fernández-Blanco et al., 2020; De Gelder et al., 2022). Using the 5-meter posting (<1 m vertical accuracy) IFSAR-DTM, we calculated topographic swath profiles, which record minimum, average, and maximum elevation values along each swath width. These individual swath profiles were then stacked perpendicular to their trend to reconstruct the lateral morphology and elevation of the CRTs. Stacked swath profiles were generated for multiple orientations and viewing angles to improve visualization and capture variations in terrace geometry.

We also conducted shoreline angle analysis on the IFSAR-DTM using TerraceM-2 (Jara-Muñoz et al., 2019) to measure shoreline angle elevation (i.e., the intersection between the paleo-reef platform and its corresponding paleo-cliff, Fig. 2) and quantitatively evaluate terrace distribution and preservation in the study area. For this, we systematically placed 100 swaths orthogonal to the trace of the paleo-cliff or the terrace inner edge, which extends continuously along the present-day shoreline. Each swath was a 200-m wide rectangular section with a variable length ranging from 1.5 to 4 km. We extracted topographic swath profiles and applied the staircase analysis function to determine shoreline angles by linearly extrapolating the paleo-reef platform and paleo-cliff slope. Linear regressions were fitted to these segments, and their intersection identified the shoreline angle position, with vertical errors derived from the 2σ confidence intervals (Jara-Muñoz et al., 2016). This method provided a quantitative framework for analyzing terrace elevation, morphology, and spatial distribution, offering insights into deformation and terrace preservation in Cape Bolinao.

3.4. Reef modelling

To explore the morphology, geometry, and possible chronology of the CRTs in Cape Bolinao, we used a kinematic profile evolution model that incorporates model parameters such as potential reef growth rate, marine erosion, initial slope, vertical land motion rate, and a chosen sea-level curve (see details in Husson et al., 2018; Pastier et al., 2019). Using the REEF code (Husson et al., 2018; Pastier et al., 2019), we produced reef simulations with parameters constrained by local observations and previous works to help us better examine and understand the reef development in Cape Bolinao since the Late Pleistocene.

We chose a representative cross-section profile that shows the best preservation of the reef terraces in Cape Bolinao. We used a potential reef growth rate (RG) of 10 mm/yr based on reported accretion rate of

10–13 mm/yr derived from Holocene reef cores in Currimao, northwest Luzon (Shen et al., 2010). The maximum reef growth depth (MRGD) was set to 30 m following Flores et al. (2023), who identified coral reefs at this depth northeast of Cape Bolinao, and the optimal reef growth depth (ORGD) and wave erosion maximum depth (WEMD) were respectively set to 2 m and 3 m (Bosscher and Schlager, 1992; Pastier et al., 2019; Chauveau et al., 2023, 2024). We used 5° as the initial slope (IS) value based on the reported inclination of the gently-sloping Sta. Cruz Formation, which serves as the basement rock of the CRTs in Cape Bolinao (Bureau of Mines and Geosciences, 1985a, 1985b). We used an erosional potential (E) of 60 mm^3/yr (Chauveau et al., 2023). For the vertical land motion value (U), we used different scenarios, with uplift rates changing between 0 mm/yr (no uplift) to 1.3 mm/yr (that is, the maximum plausible uplift rate based on the predicted age of the highest terrace MIS 5e, as reported in literature). Our simulations show that uplift rates exceeding 1.3 mm/yr result in terrace elevations inconsistent with present-day morphology, helping constrain the upper bounds of realistic uplift values. Finally, we model eustatic sea-level changes using five different sea-level curves: Waelbroeck et al. (2002), Bintanja et al. (2005), Grant et al. (2014), Rohling et al. (2009), and Spratt and Lisiecki (2016).

4. Results

4.1. Geomorphology and composition of Cape Bolinao reef terraces

The analysis of high-resolution topographic data allowed us to delineate nine paleo-reef platforms and associated paleo-cliffs in Cape Bolinao, herein named Terrace I (TI) to Terrace IX (TIX), from lowest to highest (Fig. 1c). We identified two generations of reef terraces based on morphology and heights of terrace cliffs: (1) the lower terraces characterized by narrow (from several meters wide to <500 m wide) terraces rising to 9 m with 2-to-3-m-high terrace cliffs (TI to TIII, terrace nomenclature following Ramos and Tsutsumi, 2010; Fig. 3) and (2) the higher terraces characterized by terrace widths of >100 m and rising from ~20 to 155 m with 10-to-30-m-high terrace cliffs (Fig. 2b). The lower terraces (TI to TIII) are measured and identified using high-resolution GNSS topographic surveys, while the higher terraces (TIV to TIX), that are best preserved along the western coast of Cape Bolinao, are delineated both in the field and from analysis of high-resolution DEMs.

The Cape Bolinao terraces exhibit characteristic reef facies, including framework components such as corals from the families of Poritidae,

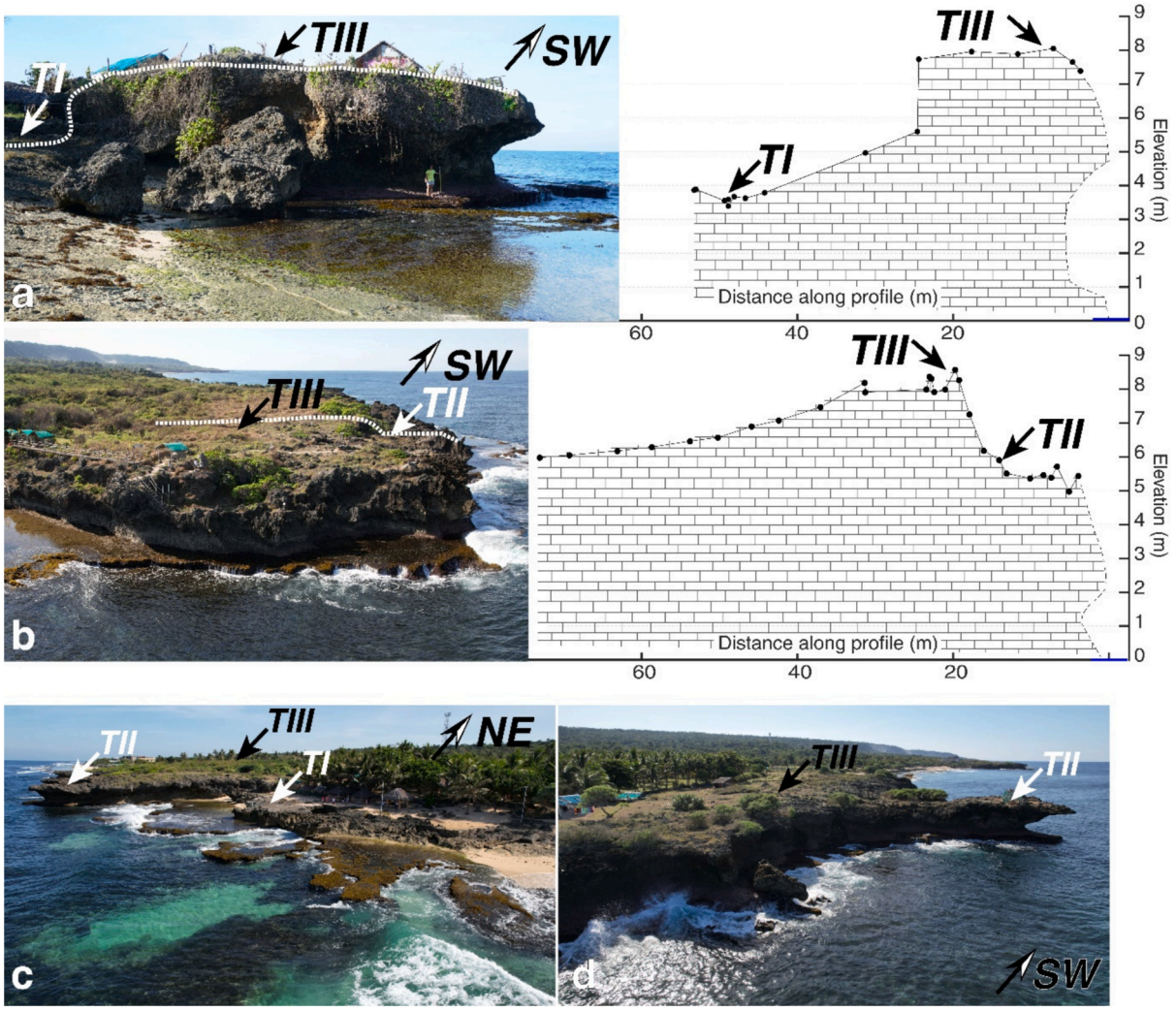

Fig. 3. Surveyed lower terraces in Cape Bolinao. We identified three steps of terraces from topographic surveys in Patar, Bolinao (location shown in Fig. 1c). **a.** Outcrop photo (white dashed line outlines survey transect) and topographic profile surveyed from Rockview Point show two steps with TI measured at 3.87 ± 0.01 m and TIII measured at 8.02 ± 0.01 m. Most of the mid-Holocene coral samples were collected from TI at this site. **b.** Field photo (white dashed line outlines survey transect) and topographic profile surveyed from Punta Piedra Point revealing two steps with TII measured at 5.72 ± 0.02 m and TIII measured at 8.57 ± 0.02 m. **c–d.** Aerial photographs illustrating the general morphology of the lower CRTs in Patar, Bolinao and their position several meters above sea level. Arrows point to the paleo-reef surfaces of identified terraces.

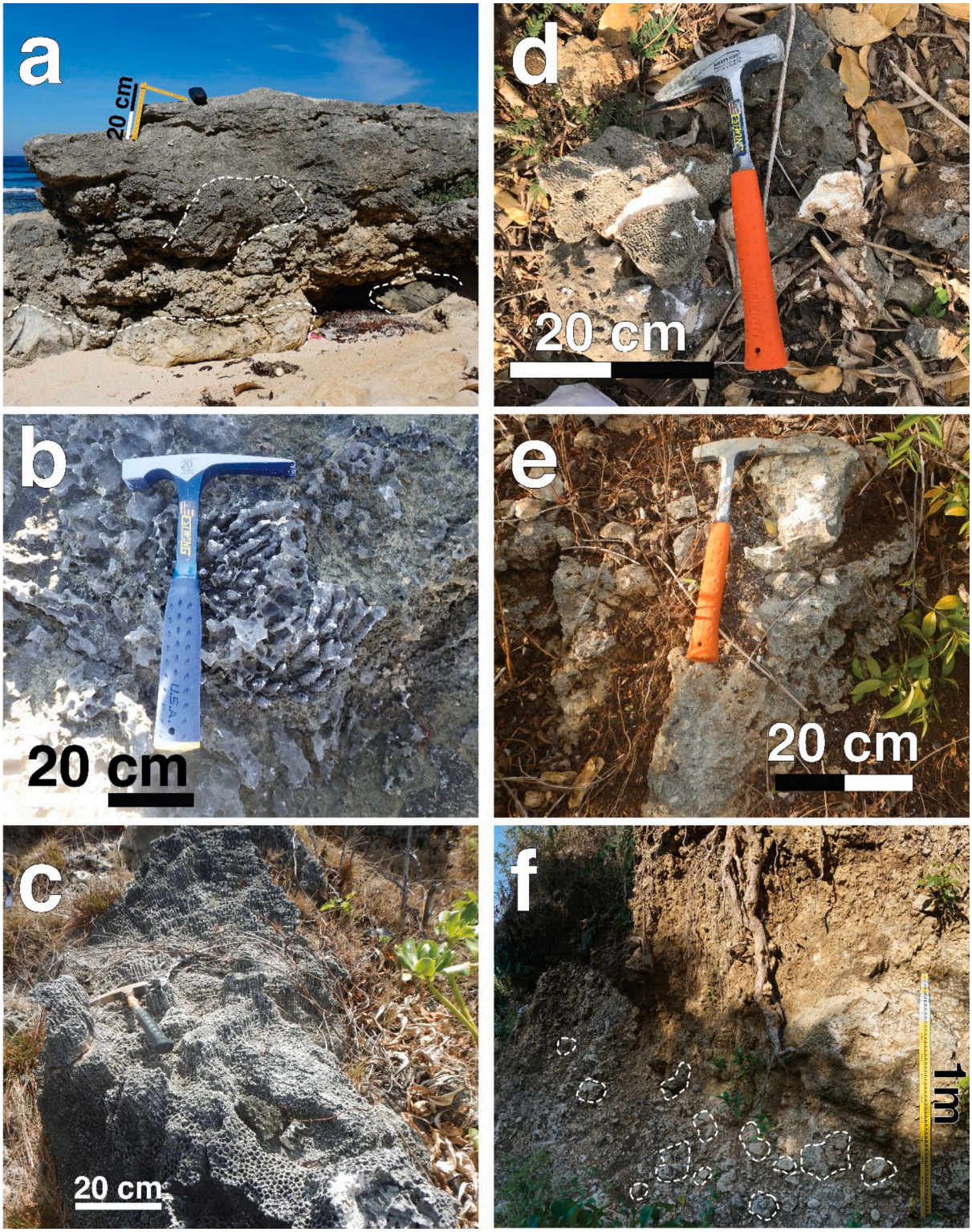

Fig. 4. Corals and composition of Cape Bolinao reef terraces. **a.** Outcrop photo of TI showing *in situ* corals (e.g., *Porites*) (bounded by white dashed contours). **b–d.** *In situ* corals from (b) TII, (c) TIII, and (d) TIX from the families of Acroporidae and Merulinidae that are diagenetically altered. **e–f.** Outcrop photos of (e) terrace TVII where we collected a *Halimeda*-rich floatstone and (f) terrace TIV, which is characterized by cobbles and boulders composed mainly by diagenetically altered corals (bounded by white dashed contours).

Merulinidae, and Acroporidae, which are commonly preserved in growth position (Fig. 4a–d). These are accompanied by skeletal fragments of corals, coralline red algae, echinoid spines, serpulids, *Halimeda* grains, lithoclasts, mollusk shells, and benthic (and encrusting) foraminifera, that can be best observed in petrographic thin sections (Supplementary Fig. 1b–g). Samples collected from reef terrace outcrops exhibit a wider range of grain-supported textures and a more diverse bioclastic assemblage, reflecting a generally higher-energy reefal depositional environment. While we recognize the importance of detailed stratigraphic analysis, time constraints and permitting

Table 1
Uranium and thorium isotopic compositions and ^{230}Th ages for coral samples by MC-ICPMS, Thermo Electron Neptune at NTU.

Sample ID	Lat.	Long.	Elev. (m)[e]	Coral sample	Ter. No.	W (g)	^{238}U 10^{-6} g/g[a]	^{232}Th 10^{-12} g/g	δ^{234}U measured[a]	[^{230}Th/^{238}U] activity[c]	^{230}Th/^{232}Th atomic ($\times 10^{-6}$)	Age (kyr ago) uncorrected	Age (kyr BP) corrected[c,d]	$\delta^{234}U_{initial}$ corrected[b]
PAT-012822-2A	119.783	16.317	3.72 ± 0.01	*P*	TI	0.22	2.4043 ± 0.0019	1501.7 ± 2.6	147.1 ± 1.4	0.06193 ± 0.00015	1634.7 ± 4.8	6.045 ± 0.017	**5.957 ± 0.019**	**149.6 ± 1.4**
PAT-012822-2B	119.783	16.317	3.56 ± 0.01	*A*	TI	0.22	2.9485 ± 0.0022	355.3 ± 2.1	144.8 ± 1.3	0.059375 ± 0.000075	8124 ± 48	5.802 ± 0.010	**5.725 ± 0.010**	**147.2 ± 1.3**
PAT-012822-2D	119.783	16.317	3.37 ± 0.01	*P*	TI	0.23	2.4486 ± 0.0020	3280.5 ± 4.6	145.1 ± 1.6	0.06620 ± 0.00021	815 ± 2.8	6.486 ± 0.023	**6.382 ± 0.028**	**147.8 ± 1.6**
PAT-012822-2E	119.783	16.317	3.52 ± 0.02	*G*	TI	0.22	2.2894 ± 0.0019	74.1 ± 2.1	142.9 ± 1.4	0.059105 ± 0.000070	30,090 ± 846	5.784 ± 0.010	**5.710 ± 0.010**	**145.3 ± 1.5**
PAT-012922-2F	119.783	16.317	3.87 ± 0.01	*G*	TI	0.24	2.1940 ± 0.0021	116.7 ± 1.9	142.9 ± 1.4	0.060198 ± 0.000076	18,665 ± 300	5.894 ± 0.011	**5.819 ± 0.011**	**145.3 ± 1.5**
PAT-012922-2G	119.783	16.317	3.87 ± 0.01	*G*	TI	0.22	2.1671 ± 0.0019	2835.9 ± 4.0	143.2 ± 1.4	0.06255 ± 0.00020	788.1 ± 2.7	6.129 ± 0.022	**6.026 ± 0.027**	**145.6 ± 1.4**
PAT-012822-3A	119.781	16.311	2.46 ± 1	*Po*	TI	0.24	2.3209 ± 0.0016	2429.1 ± 3.4	145.5 ± 1.3	0.05893 ± 0.00017	928.4 ± 2.8	5.753 ± 0.018	**5.656 ± 0.022**	**147.9 ± 1.3**
PAT-012822-3E	119.781	16.311	2.46 ± 1	*Ar*	TI	0.26	2.8897 ± 0.0025	109.4 ± 1.8	146.8 ± 1.4	0.053937 ± 0.000066	23,492 ± 387	5.2483 ± 0.0094	**5.174 ± 0.009**	**148.9 ± 1.4**

Analytical errors are 2s of the mean.
Coral Sample: P = *Porites* sp., A = *Acropora* sp., G = *Goniastrea* sp., Po = *Porites* sp. (overturned), Ar = *Acropora* sp. (reworked). W: Weight (g).
[a] $[^{238}U] = [^{235}U] \times 137.77$ (±0.11 ‰) (Hiess et al., 2012); $\delta^{234}U = ([^{234}U/^{238}U]_{activity} - 1) \times 1000$.
[b] $\delta^{234}U_{initial}$ corrected was calculated based on ^{230}Th age (T), i.e., $\delta^{234}U_{initial} = \delta^{234}U_{measured} \times e^{\lambda 234 \times T}$, and T is corrected age.
[c] $[^{230}Th/^{238}U]_{activity} = 1 - e^{-\lambda 230T} + (\delta^{234}U_{measured}/1000)[\lambda_{230}/(\lambda_{230} - \lambda_{234})](1 - e^{-(\lambda 230 - \lambda 234)T})$, where T is the age. Decay constants are 9.1705×10^{-6} yr^{-1} for ^{230}Th, 2.8221×10^{-6} yr^{-1} for ^{234}U (Cheng et al., 2013), and 1.55125×10^{-10} yr^{-1} for ^{238}U (Jaffey et al., 1971).
[d] Age corrections, relative to 1950 CE, were calculated using an estimated atomic $^{230}Th/^{232}Th$ ratio of 4 (± 2) $\times 10^{-6}$ (Shen et al., 2008).
[e] Measured elevations and uncertainties of coral samples are reported in m amsl. Elevations of reworked samples were derived from IFSAR-DTM with vertical accuracy of <1 m.

Table 2
Radiocarbon ages for carbonate samples by NEC accelerator mass spectrometers and 4 Thermo IRMSs at Beta.

Sample ID	Latitude	Longitude	Elevation (m)	Coral sample	Terrace number	Measured radiocarbon age (BP)	IRMS $\delta^{13}C$ (‰)[b]	Conventional radiocarbon age (BP)[a]	Calendar calibration (95.4 % probability)[c,d,e]
PAT-012822-2A	119.783	16.317	3.72 ± 0.01	*Porites* sp.	TI	5240 ± 30	−5.0	5570 ± 30	6.263–5.862
PAT-012822-2B	119.783	16.317	3.56 ± 0.01	*Acropora* sp.	TI	4920 ± 30	−1.0	5310 ± 30	5.960–5.564
PAT-012822-2E	119.783	16.317	3.52 ± 0.02	*Goniastrea* sp.	TI	4800 ± 30	−1.3	5190 ± 30	5.862–5.447
PAT-012822-2C	119.783	16.317	3.37 ± 0.01	*Tridacna* sp.	TI	41,350 ± 730	+2.2	41,790 ± 730	45.300–42.912
PAT-012822-1A	119.782	16.317	6.82 ± 0.01	*Tridacna* sp.	TIII	41,720 ± 780	+2.2	42,160 ± 780	45.779–43.057

[a] The "Conventional Radiocarbon Age" was calculated using the Libby half -life (5568 years), is corrected for total isotopic fraction and was used for calendar calibration where applicable. The Age is rounded to the nearest 10 years and is reported as radiocarbon years before present (BP), "present" = 1950 CE.
[b] The reported IRMS $\delta^{13}C$ (‰) values were measured separately in an IRMS (isotope ratio mass spectrometer).
[c] OxCal version 4.4 (Bronk Ramsey, 2009) was used to calibrate conventional radiocarbon ages using the MARINE20 Marine Radiocarbon Age Calibration Curve (Heaton et al., 2020).
[d] We used local DeltaR = –262 ± 63 based on coupled ^{230}Th and ^{14}C ages of three coral samples from Cape Bolinao calculated using an online application for DeltaR calculation (Reimer and Reimer, 2017).
[e] Calendar-calibrated radiocarbon (^{14}C) ages are reported in kyr cal BP, with a 95.4 % probability range (± 2σ).

limitations (i.e., COVID restrictions), prevented us from conducting comprehensive stratigraphic section logging during fieldwork. Despite these challenges, we were able to make targeted observations and collect samples from key outcrops, especially above the Holocene sequences, which informed our interpretations of reef terrace development.

Petrographic analysis of samples collected from higher terraces TIV to TIX (Supplementary Fig. 1b–g) reveal dominant components such as coral fragments, *Halimeda*, benthic foraminifera, gastropods, and lithoclasts set in micritic to microsparitic matrices and show a range of textures from packstone to grainstone/rudstone. Samples from higher terraces (TIV–TIX) display extensive diagenetic overprinting (e.g., widespread replacement of aragonite by blocky or drusy calcite spar, micritic alteration, neomorphism, pedogenic features) that reflects prolonged subaerial exposure and associated carbonate dissolution and cementation under near-surface meteoric conditions. In samples collected from terraces TII to TIX, many aragonitic components (including coral skeletons) exhibit diagenetic alteration, where original textures and porosity have been replaced and filled by blocky calcite spar, or in some cases, have been dissolved leaving molds (Supplementary Fig. 2). In the sections below, we describe each terrace in detail, focusing on its geomorphic expression and lithologic composition.

The lowest terrace, TI, is best observed in Rockview Point at a measured elevation of 3.87 ± 0.01 m and is characterized by a width of 5–10 m (Fig. 3a). It is limited seaward by gently sloping sand-covered beach deposits and it transitions gradually into the sand-covered terrace TII/TIII. The paleo-reef surface of TI is characterized by *in situ* massive and branching corals from the families of Poritidae, Merulinidae, and Acroporidae. Coral samples, composed of aragonite skeleton with little to no evidence of diagenesis, yielded ^{230}Th ages of 6.38–5.71 kyr BP and radiocarbon ages of 6.26–5.45 kyr cal BP (Tables 1 and 2, Supplementary Fig. 2a–b). The *Porites* and *Acropora* corals yielded relatively older ages compared to *Goniastrea* corals with $\delta^{234}U$ initial values (Table 1) within the acceptable limits (145 ± 5 ‰, see Chutcharavan et al., 2018). In Punta Piedra, TI is composed of beachrock with abundant large benthic foraminifera (e.g., Calcarinidae), gastropods, and reworked pristine *Porites* (PAT-012822-3A) and *Acropora* (PAT-012822-3E) corals dated 5.66 and 5.17 kyr BP, respectively. A *Tridacna* shell collected from TI yielded a radiocarbon age of 45.3–42.91 kyr cal BP, potentially indicating reworking of older material or exposure of an older substrate (Table 1).

The second terrace, TII, is best recognized discontinuously along rocky exposures on the coast and is regularly subjected to sea sprays especially during high-energy wave conditions. Along the profile in Punta Piedra Point (Fig. 3b), TII is characterized by a rocky jagged surface with a measured elevation of 5.72 ± 0.02 m and a narrow width of <20 m. It is limited to the sea by rocky almost vertical cliffs and it is limited landward by meter-high terrace risers of TIII. Branching corals, already influenced by diagenesis, are observed on the terrace surface (Fig. 4b). Where observed, tidal notches are etched on the vertical cliffs of TII/TIII exposed to the sea. In our survey sites, the retreat point (2–3 m depth) of tidal notches was observed to coincide with elevation of the identified TI surface (Fig. 3). Fossil corals from this terrace exhibit clear signs of diagenetic alteration, and no pristine coral samples suitable for dating were recovered (Supplementary Fig. 2c–d).

We identified TIII terrace at a measured elevation of 8.57 ± 0.02 m (rising to about 14 m based on DEM-derived shoreline angle analysis). This is the widest Holocene terrace, with a width of 200 to 500 m and follows the coastline for >10 km. TIII is better preserved along the northwest-facing side of the coast. The terrace surface is highly vegetated with occasional outcropping rocks and is highly modified, as the area is transformed by coastal developments. Along the profile in Punta Piedra Point (Fig. 3b), the terrace is characterized by a rocky surface dominated by *in situ* massive and branching corals from the families of Poritidae, Merulinidae, and Acroporidae that are diagenetically altered (Fig. 4c, Supplementary Fig. 2e–f). Because of the high degree of diagenesis observed on the corals from this terrace, we found no coral material suitable for radiometric dating. A *Tridacna* shell collected from the surface of TIII yielded a radiocarbon age of 45.78–43.06 kyr cal BP, possibly representing reworked older reef material incorporated into the younger terrace deposits (Table 1).

The fourth terrace, TIV, has a mean elevation of 31 ± 14 m and is characterized by terrace width of 0.1 to 1 km, which increases from west to north. The surface of TIV is dissected by several drainage systems. Outcrop exposures reveal that this terrace is composed of abundant subrounded to sub-angular diagenetically altered coral rubble and boulders within a sandy matrix (Fig. 4f, Supplementary Fig. 1e). Petrographic description of an outcrop sample reveals abundant angular to subrounded lithoclasts (e.g., *Halimeda* floatstone, bored coral fragments,

and skeletal packstone) and broken fragments of benthic foraminifera, coralline red algae, and echinoid plates are also present (Supplementary Fig. 1e).

Terrace TV is at elevation of 55 ± 15 m is characterized by terrace width of 0.5 to 1.8 km which increases from west to north. Petrographic analysis of an outcrop sample from this terrace shows a grain-supported fabric composed predominantly of large benthic foraminifera (e.g., *Amphistegina, Calcarina*) with subordinate mollusks, gastropods, and minor red algae. Situated at an elevation of 81 ± 13 m, terrace TVI has a width of ~0.1 to 0.3 km increasing towards the northeast. Petrographically, gastropods and random sections of large benthic foraminifera (e.g., *Calcarina*) are abundant in an outcrop sample from this terrace (Supplementary Fig. 1d). Coral fragments are encrusted by coralline red algae and acervulinid foraminifera and aragonite skeleton is replaced by calcite spar.

The seventh terrace, TVII, is at an elevation of 102 ± 10 m and has a terrace width of 0.2 to 3 km increasing from southwest to northeast. It is highly dissected along the northern portion of the cape where it is the widest and is better preserved along the northwest- to north-facing sides of the coast (Fig. 1c). Along the western coast, its outer edge is marked by alternating ridges and channels, that are reminiscent of spurs and grooves presently observed along the modern reef edge. Petrographic description of a sample collected from along the profile reveals *Halimeda*-rich floatstone with random sections of benthic foraminifera and other skeletal components in micritic matrix (Fig. 4e, Supplementary Fig. 1c). *Halimeda* fragments are enveloped by thin micrite rim then filled by calcite spar. Terrace TVIII has a narrow width (~0.1 to 0.3 km) and a mean elevation of 120 ± 14 m. A sample from a small outcrop reveals a poorly sorted, grain-supported skeletal packstone dominated by *Halimeda* segments, benthic foraminifera (e.g., *Amphistegina,*

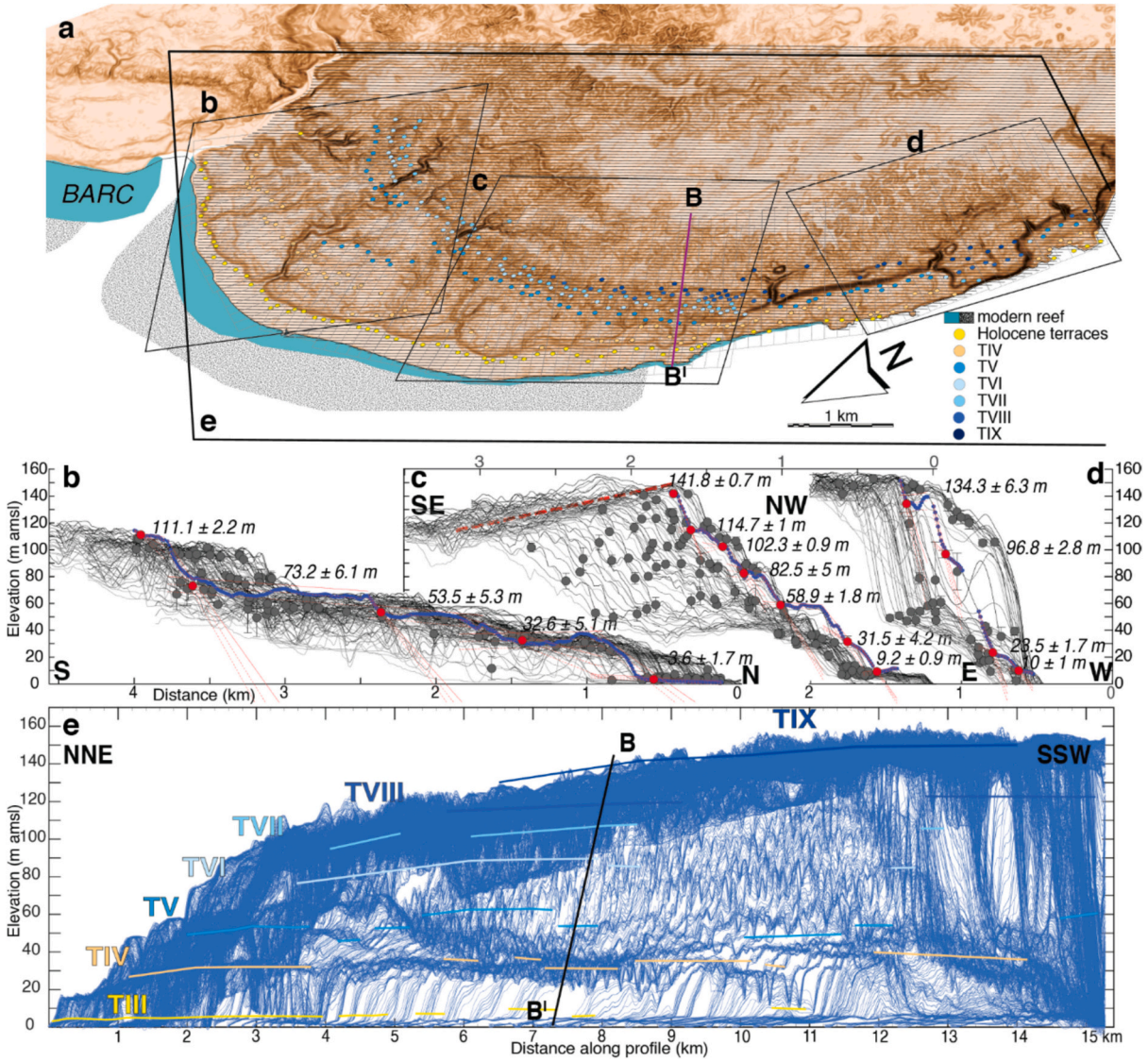

Fig. 5. Morphology and deformation pattern of Cape Bolinao CRTs. **a.** Slope map of Cape Bolinao CRTs with the location of the 100 swaths we used for the shoreline angle analysis (in boxes b, c, d) and the ~230 parallel lines we used to calculate the stacked swath profiles (in box e). **b–d.** Shoreline angle analysis for the (b) northern portion of the cape with cross section from S-N, (c) central portion (northwest-facing side) showing higher terraces tilted towards the SE direction (red dashed line), (d) southern portion with cross section from E-W. Gray lines represent the topographic swaths (horizontal distance in km) calculated using TerraceM while the gray circles represent the elevation and position of delineated shoreline angles with vertical uncertainties. A representative profile is shown highlighted by blue and red (shoreline angles) circles. **e.** Representative stacked swath profiles generated in Cape Bolinao (view looking ESE with interpretation of CRT levels). The highest terrace, TIX, is generally observed along the central and southern portion of the cape and is characterized by a broad, generally planar paleo-reef surface. Also prominent is the general flat morphology of the reef terraces which are gently sloping down towards the NE to where the modern reefs are presently observed to be widest. Colored lines highlight the approximate delineation of the mapped terraces (TIII to TIX).

Heterostegina), fragments of red calcareous algae and encrusting foraminifera, and echinoderm spines, gastropods, and molluscan fragments. Most skeletal grains are surrounded by thin micrite envelopes and ~ 10 % moldic porosity is observed.

The highest reef platform, TIX, is a broad, generally planar paleo-reef surface with terrace width of ~5 km and ranges in elevation from 130 to 155 m (with a mean elevation of 143 ± 12 m). The DEM shows its surface to be highly dissected, with circular depressions, possibly sinkholes (Fig. 1c). Diagenetically altered corals from the families of Poritidae and Merulinidae were recognized on this terrace (Fig. 4d). Because of the high degree of diagenesis of the samples, we found no material suitable for radiometric dating (Supplementary Fig. 2g–h). Petrographically, outcrop samples identified as coral rudstone to packstone reveal corals as major components while gastropods, benthic foraminifera (*Amphistegina*, *Calcarina*), encrusting foraminifera, coralline red algae, echinoid spines, and serpulids were minor (Supplementary Fig. 1b). Terraces TVIII and TIX are generally preserved along the west-facing side of the coast from the central to the southern portion of the cape.

4.2. Terrace deformation in Cape Bolinao

To examine the lateral extent and large-scale morphology of the CRTs in Cape Bolinao, we generated stacked swath profiles and we tracked shoreline angles (Fig. 5), revealing slight variability in terrace elevations from north to south. Overall, the CRTs gently slope downward towards the northeast, where the Bolinao-Anda Reef Complex (BARC) is most extensive and well-preserved (Fig. 5e). We also observed a lateral pattern in terrace preservation, with terraces TVIII-TIX better preserved along the southwest and terraces TV to TVII more prominent in the northeast. TIV exhibits a poorly developed terrace topography, likely due to its composition of predominantly coral boulders and cobbles, resulting in irregular terrace surfaces. In addition, the number of terraces varies, with fewer terraces preserved in the southwest compared to the central portion of the cape, particularly along the west-northwest-facing coastline.

The gentle northeastward slope of the CRTs is hypothesized to be influenced by antecedent topography, with the modern BARC located in the northeastern portion of the Cape. Notably, CRTs in the north are wider than those in the west, likely due to greater accommodation space in the northern region. In Cape Bolinao, accommodation space and antecedent topography—shaped by factors such as vertical uplift rate, initial basement slope, reef growth rate, marine erosion, and sea-level fluctuations—play a critical role in influencing CRT architecture (Maxwell, 2024). This indicates that pre-existing topographic variations strongly impacted terrace development and morphology in the study area. While the presence of a large river in the north and potential local faulting may also contribute to this pattern, exploring their interactions with CRT morphology and development is beyond the scope of this paper.

Our analysis reveals that while the Cape Bolinao CRTs exhibit an overall northeastward dip, the higher terraces (TVIII-TIX) show a distinct ESE-ward tilt. This observation, derived from multi-directional stacked swath profile comparisons, aligns with the eastward tilt direction previously reported by Maemoku and Paladio (1992) for the highest CRT. To better constrain deformation patterns, we systematically analyzed ~390 shoreline angles, which confirmed both the lateral variability in terrace preservation and the ESE-ward directed tilt of TVIII-TIX initially revealed through the stacked swath profiles (Fig. 5c; Supplementary Fig. 3). Lower terraces (TVII and below; Fig. 5b) meanwhile show no evidence of this tilt, highlighting a clear contrast in deformation history between the upper and lower CRT sequences. This ESE-ward directed tilt may be interpreted as localized tectonic deformation (e.g., fault-related uplift or tilting), though the exact driver requires further study. Our combined swath profile and shoreline angle analyses also reveal that Holocene terraces fringe the entire coast from northeast to southwest, though with notable elevation variations. The elevations derived from stacked swath profile and shoreline angle analyses are consistent with our field measurements, further supporting these findings.

4.3. Reef sequence models

By taking into consideration different parameters (i.e., sea-level curve, vertical uplift, reef growth rate, erosion rate, initial substrate slope, see Table 3), we can infer the conditions which supported the development of the current morphology of the terraces. We used the elevation and width of the CRTs derived from our high-resolution geomorphic analysis and directly compared it with the reef simulations produced. We selected cross-section profile B-B^{I} from the central portion of Cape Bolinao as our representative profile because it displays the most complete and best-preserved CRT sequence, unlike the northern and southern portions, where poor preservation limits profile selection. We superimposed it with stacked swath profiles calculated parallel to its orientation. Although the Cape Bolinao CRTs demonstrate a general gentle dip towards the northeast, local elevation variability occurs along strike. To minimize uncertainties, we chose this representative profile with optimal terrace preservation and minimal deformation, used stacked swath profiles to establish regional trends, and incorporated approximately 390 shoreline angles for robust analysis. Different profile choices, particularly those with varying orientations or characteristics, could affect modelling results; however, the extent of this effect would need to be evaluated in future works. For our reef models, we explored the parametric fields of sea level and uplift and used constant values (based on local observations and previous works) for the rest of the parameters. By focusing our attention on these parameters, we can examine the effects of late Quaternary sea-level variations and changes in vertical uplift in the development of the CRTs in the region.

Since we did not assign an age to TIX *a priori*, our approach focused on present-day terrace morphology, specifically elevation and width, and used reef modelling to explore a range of uplift rates capable of reproducing these features. The resulting simulations then informed the inferred ages of the terraces. To reproduce the maximum terrace elevation at 155 m amsl, uplift rates should be >0.4 mm/yr irrespective of the sea-level curves used. However, given the lateral extent of the Cape Bolinao CRTs, low uplift rates are not enough to reproduce the terrace width of ~5 km for the highest paleo-reef surface, TIX. We then use higher uplift rates (>1.10 mm/yr) to increase the reef terrace

Table 3
Model input parameters and values used.

Input parameter	Acronym used	Values used	Reference
Potential reef growth rate	RG	10 mm/yr	Shen et al. (2010)
Initial slope	IS	5°	Bureau of Mines and Geosciences (1985a, 1985b)
Potential erosion rate	E	60 mm^3/yr	Chauveau et al. (2023)
Vertical land motion (Uplift)	U	0 mm/yr to 1.3 mm/yr	This Study
Maximum reef growth depth	MRGD	30 m	Flores et al. (2023)
Optimal reef growth depth	ORGD	2 m	Bosscher and Schlager (1992); Chauveau et al. (2023, 2024)
Wave erosion maximum depth	WEMD	3 m	Pastier et al. (2019); Chauveau et al. (2023, 2024)
Sea-level curves used	SL	W02; B05; R09; G14; SL16	Waelbroeck et al. (2002), Bintanja et al. (2005), Rohling et al. (2009), Grant et al. (2014), and Spratt and Lisiecki (2016).

widths. Higher uplift rates also produce terraces above 155 m. In Cape Bolinao, the highest terrace is situated at 155 m and no terraces above it are presently observed. With these restrictions, uplift rates of 1.15–1.20 mm/yr were used to achieve TIX terrace elevation at 155 m amsl with minimum width of 1 km. Based on these constraints, we adopted a best-fitting uplift rate of 1.17 ± 0.03 mm/yr, which consistently generates a terrace at ~155 m with appropriate width. Under this uplift rate value, the modelled terrace, TIX, corresponds to MIS 5e regardless of the sea-level curves used (Fig. 6). Meanwhile, the lowest terrace in our simulations, situated near present sea level and with widths of 0.5 to 1 km, corresponds to MIS 1 and is supported by radiometric age data.

5. Discussion

5.1. Cape Bolinao CRT development during the Late Pleistocene

As highlighted by previous works (e.g., De Gelder et al., 2020; Chauveau et al., 2024), different sea-level curves shape different CRT morphologies; hence, the choice of the sea-level curve will most likely determine the overall fossil reef morphology. Because of this, we ran our simulations and tested five different sea-level curves: Waelbroeck et al. (2002), Bintanja et al. (2005), Grant et al. (2014), Rohling et al. (2009), and Spratt and Lisiecki (2016) to reproduce the coral reef sequences in Cape Bolinao. Comparing the simulations produced, we find the sea-level curve of Waelbroeck et al. (2002) to closely reproduce the elevations of the reef terraces we observe today. This curve is based on North Atlantic and Equatorial Pacific Ocean benthic foraminifera oxygen isotopic ratios calibrated with relative sea-level data based on corals over the last climatic cycle. The other sea-level reconstructions were meanwhile based on a global compilation of benthic oxygen isotope data (Bintanja et al., 2005), on oxygen isotopic ratios of planktonic foraminifera and bulk sediment from the Red Sea (Rohling et al., 2009), on U/Th-dated speleothem oxygen isotopic ratio record synchronized with an Asian monsoon signal with dust and SL records (Grant et al., 2014), and on the principal component analysis of earlier compilations (Spratt and Lisiecki, 2016).

The best-fitting simulation is obtained using the sea-level curve of Waelbroeck et al. (2002) and an uplift rate of 1.17 mm/yr (Fig. 7). In general, the reef simulation clearly replicated the TIX terrace at an elevation of ~155 m and the elevations of the fringing terraces (TVII to TIV). In terms of terrace widths, it showed relatively wider (>0.5 km) planar surfaces for TIX, TVII, and TIV and narrow (<300 m) terrace surfaces for TVIII and TVI, which is in agreement with our morphological analysis. The modelled morphology and width of terrace TV, however, is at odds with our morphological analysis. It is worth noting that, while the reef simulation also produced terraces at elevations higher than 160 m, we did not observe any terraces higher than 155 m in Cape Bolinao. Also, it did not fully reproduce the width of TIX (~5 km), that we observe today. To explain this, we refer to the underlying lithologic units (interpreted to indicate an epi- to upper meso-pelagic setting) beneath the reefal terraces of Cape Bolinao. We postulate that a relative sea-level change (~200–300 m) is needed to reduce paleo-water depths and subsequently provide a suitable substrate for later shallow-marine reef development. The gently-dipping beds provided more

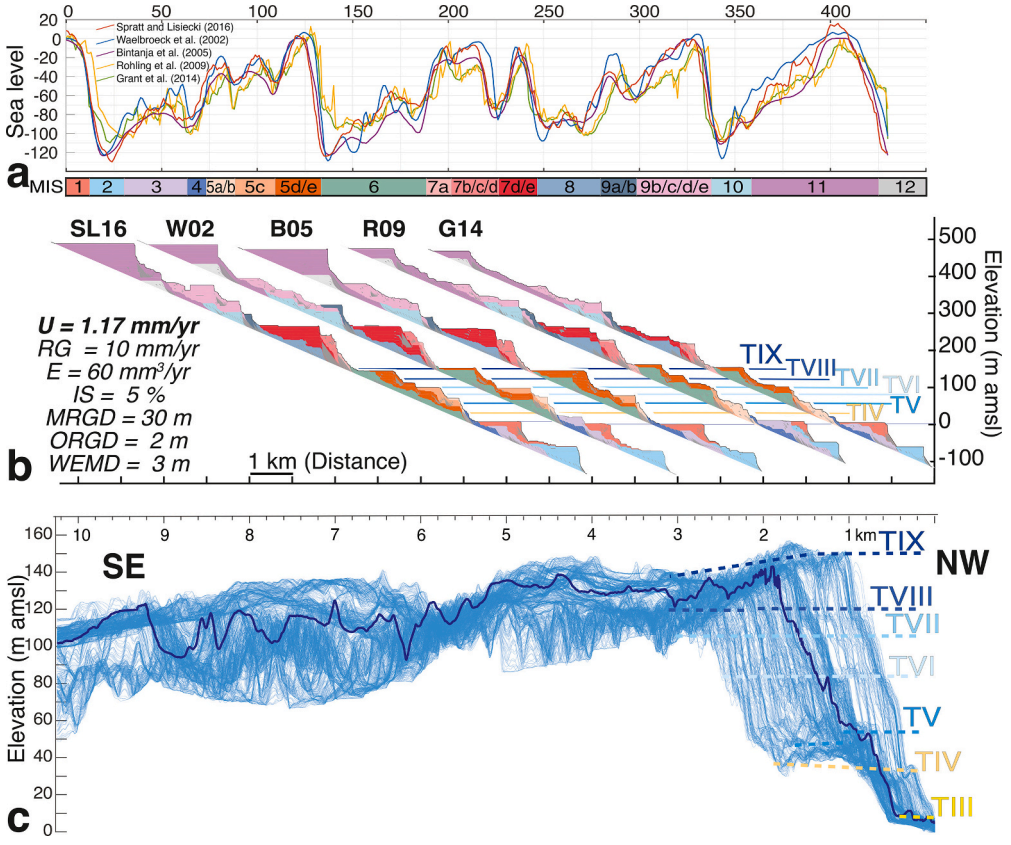

Fig. 6. Reef modelling results for the Cape Bolinao CRTs using different sea-level curves and constant parameters. **a.** Sea-level curves used to reproduce the CRTs in Cape Bolinao. The color codes below indicate the Marine Isotope Stages (MIS) from MIS 1 to 11. **b.** Reef simulations reproduced using different sea-level reconstructions. The paleo-reef terraces for TIX and TIV are highlighted by colored lines and model parameters are also shown. **c.** Representative stacked swath profile along the central portion of the coast where a complete suite of CRTs was observed. For comparison, shown here is the general topography showing the elevations of the CRTs along the best-preserved area in Cape Bolinao. SL16: Spratt and Lisiecki (2016), W02: Waelbroeck et al. (2002), B05: Bintanja et al. (2005), R09: Rohling et al. (2009), G14: Grant et al. (2014), U: Uplift (Vertical land motion rate), RG: Potential reef growth rate, E: Erosion rate, IS: Initial slope, MRGD: Maximum reef growth depth, ORGD: Optimal reef growth depth, WEMD: Wave erosion maximum depth.

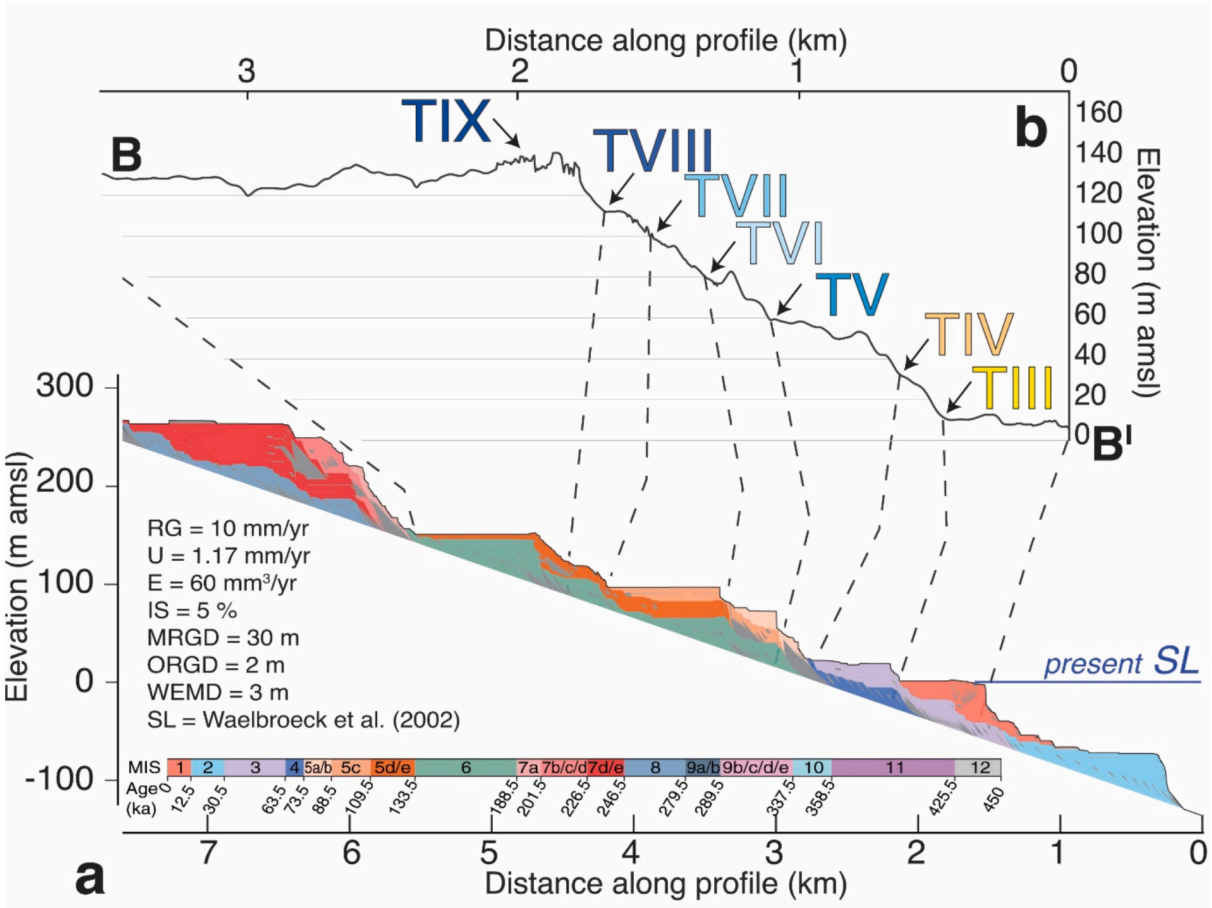

Fig. 7. Best-fit reef simulation. **a.** Reef simulation using the sea-level reconstruction of Waelbroeck et al. (2002) and uplift rate of 1.17 mm/yr. **b.** Representative topographic profile (B-B^{I}, Fig. 1c) measured along the central portion of the cape where a complete suite of terraces is observed. Dashed lines allow comparison of the field observations with the corresponding modelled terraces and arrows point to the shoreline angles calculated along this profile. RG: Potential reef growth rate, U: Uplift (Vertical land motion rate), E: Erosion rate, IS: Initial slope, MRGD: Maximum reef growth depth, ORGD: Optimal reef growth depth, WEMD: Wave erosion maximum depth, SL: Sea-level curve used.

accommodation space for the development of an extensive Late Pleistocene reef platform or table reef. Continuous uplift superimposed on a changing sea level led to the emergence of this table reef followed by formation of fringing reefs (corresponding to lower reef terraces) along its slope. Husson et al. (2018) pointed out that relative sea-level change (uplift or subsidence) exposes pristine domains of the shore to reef growth and expands the accommodation space. Vertical land motion therefore fosters reef carbonate productivity, and, in addition, productivity is higher for shallow slopes than for steep ones as the former provide wider accommodation spaces, which can provide favorable foundations for reef growth during subsequent reoccupations (Husson et al., 2018; Pastier et al., 2019).

With our best-fitting simulation, we can propose a morpho-chronological framework for the Cape Bolinao CRTs, with TIX formed at peak MIS 5e, and the lowest terrace (corresponding to TI to TIII) formed during MIS 1. The reef simulations reproduce two terraces (a well-defined planar surface and an indistinct lower terrace) for MIS 5e and MIS 5a. Sea-level reconstructions for the MIS 5e show either a single peak (Waelbroeck et al., 2002; Bintanja et al., 2005; Grant et al., 2014) or multiple peaks (Rohling et al., 2009). Our numerical reef simulations reveal that at least two terraces can be created during MIS 5e using the curves of Spratt and Lisiecki (2016), Waelbroeck et al. (2002), and Bintanja et al. (2005) while three terraces can be reproduced using the curves of Grant et al. (2014) and Rohling et al. (2009). The simulations suggest that more than one terrace can be created during MIS 5e and multiple sea-level peaks are not required to create such terraces within one isotopic stage. Our results are comparable with the findings of Chauveau et al. (2023) and De Gelder et al. (2023) from their works in Sumba Island in which their simulations show that a single peak during MIS 5e can form multiple terraces associated with MIS 5e. We also propose that the antecedent topography (the terraces which formed during MIS 6) influenced the pattern and morphology of the overlying MIS 5e terraces as former terraces were reoccupied during the MIS 5e transgression (Fig. 7). For Sumba Island CRTs, Chauveau et al. (2023) showed that antecedent CRTs influence new reef constructions and more likely explain the presence of multiple CRTs associated with MIS 5e. The results of our reef modelling support the proposition of Pastier et al. (2019) challenging the commonly assumed bijective relationship between sea-level highstands and terraces (that is, one-to-one correspondence between a reef terrace and a sea-level highstand).

5.2. *Tectonic deformation along the Manila Subduction Zone*

With our detailed morphological analysis coupled with reef modelling, we determine that the most likely long-term uplift rate is 1.17 ± 0.03 mm/yr for Cape Bolinao. This value is comparatively lower than previously estimated by Maemoku and Paladio (1992) in Cape Bolinao (1.3 mm/yr) and higher than MIS 5e uplift rates estimated by Maxwell et al. (2018) from CRTs in northwest Luzon (0.13 to 0.3 mm/yr). We observed the highest reef platform (MIS 5e reef) to be tilted towards the ESE and the paleo-reef surfaces are striking towards the NNE. The deformation patterns observed as well as the high uplift rates estimated

are more likely attributed to subduction processes along the Manila Trench. In particular, the subduction of the Scarborough Seamount Chain (SSC), a NE-striking South China Sea extinct spreading ridge, beneath the west Luzon forearc region (e.g., Pautot and Rangin, 1989; Armada et al., 2020) likely drives both the elevated uplift and the observed tilting in Cape Bolinao.

Differential uplift, where proximal areas near the SSC subduction front experience higher uplift rates compared to more distal sites, could be explained by localized deformation brought about by SSC subduction (Armada et al., 2020). The documented ESE tilt of the highest reef terraces and the along-strike variability in CRT elevations reflect a complex interplay of tectonic forces along subduction margins influenced by oceanic asperities (e.g., Dominguez et al., 1998; Wang and Bilek, 2011). As oceanic asperities subduct, the margin adapts to the underthrusting topography resulting in the deformation of the upper plate (e.g., Dominguez et al., 1998). Consequently, a subducting seamount or ridge generates a complex network of fractures fostering localized uplift, tilting, and block rotation, even in the absence of large earthquakes (Wang and Bilek, 2011).

Based on analyses of seismic reflection data and bathymetric data, Armada et al. (2020) provided new evidence of bathymetric highs (i.e., seafloor relief related to seamounts and ridges) being subducted eastward beneath the Luzon Island with vertical deformation in the forearc region being concentrated at 17°N to 15.5°N latitudes. Our work provides a supporting evidence of SSC subduction beneath the west Luzon forearc during the late Quaternary causing high uplift in the region and tilting of the highest reef terrace towards the ESE. Consequently, this might also explain the difference in long-term uplift rates estimated from the CRTs in Cape Bolinao and in northwest Luzon.

The Luzon forearc basin can be separated into the North Luzon Trough (NLT) and the West Luzon Trough (WLT) with boundary at the 17°N latitude (Fig. 1b, Armada et al., 2020) and Hsu et al. (2012) suggests a partially locked fault zone near 15–16.5°N beneath the WLT adjacent to SSC. While the CRTs of Cape Bolinao are situated in this highly coupled region, the CRTs of northwest Luzon are adjacent to the NLT, characterized by a relatively smooth seafloor. By examining the relationship between observed coastal late Pleistocene uplift rates and various geodynamic parameters, Henry et al. (2014) suggests that the first order parameter explaining coastal uplift along subduction zones is the small-scale heterogeneities of the subducting plate (i.e., subducting aseismic ridges). With this, we suggest that roughness of the seafloor (i.e., the impinging SSC) might likely be the reason for the difference in long-term uplift rates between the two regions.

The subduction of SSC might also be the likely explanation on the variation of mid-Holocene coral ages collected from the lower terraces from both localities. The younger mid-Holocene corals in Cape Bolinao (This Study; Ramos and Tsutsumi, 2010) might have experienced a more recent uplift compared to the relatively older mid-Holocene corals in northwest Luzon (Fig. 8, Table 4). In addition, the older corals in northwest Luzon (i.e., Currimao, Badoc; see Maeda et al., 2004; Shen et al., 2010; Maxwell et al., 2018) are better preserved than those in Cape Bolinao as we did not find pristine corals in our sites older than 6.4 kyr. It may be the case that the corals in Cape Bolinao have been more affected by meteoric diagenesis than the ones in northwest Luzon. While high uplift rates explain much to this as the reefs may be subaerially exposed earlier and longer, the presence of submarine groundwater discharge in Cape Bolinao (Cantarero et al., 2019) might also contribute.

6. Conclusions

This work presents a new interpretation of the formation of CRTs in the northern Coral Triangle as a function of relative sea-level changes and tectonic uplift along an active margin during the late Quaternary (since ~130 kyr). With new geochronologic data coupled with high-resolution morphological analysis and reef stratigraphic numerical modelling, we examine in detail the Cape Bolinao CRTs in western Luzon, Philippines and provide a record of sea-level changes in the West Philippine Sea during the last glacial cycle. We estimate a new average

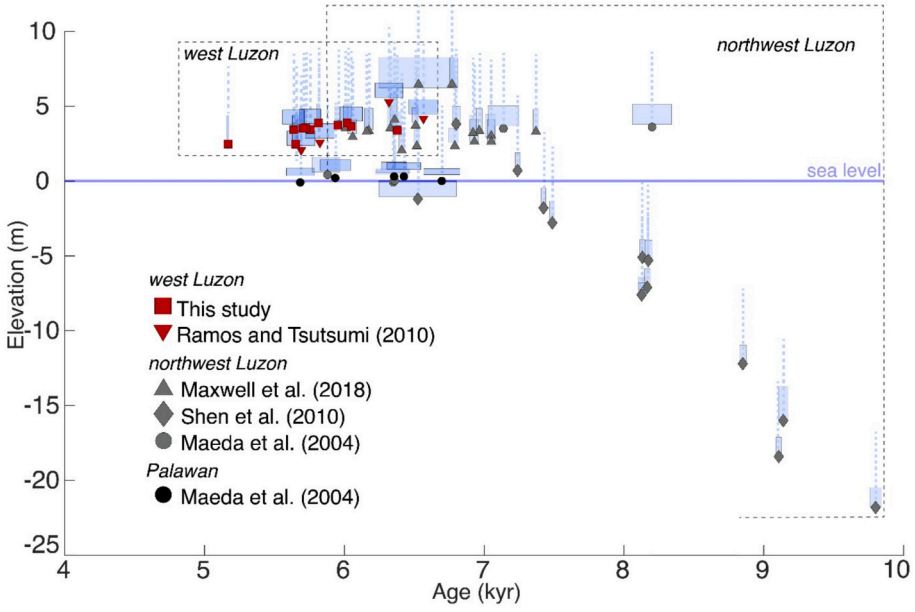

Fig. 8. Elevation of dated fossil Holocene corals in west Luzon and northwest Luzon. Plotted are the elevation and ages of dated Holocene corals (plotted as symbols) collected along west Luzon Island. The symbols represent the coral ages reported by previous works in Pangasinan (Ramos and Tsutsumi, 2010, in inverted triangle), in Currimao (Shen et al., 2010, in diamond symbols), in Currimao and Badoc (Maxwell et al., 2018, in triangle symbols), and in Currimao, Badoc, and Palawan (Maeda et al., 2004, in circles). Shen et al. (2010) examined reef cores thereby providing an older, longer record for the Holocene reef development in northwest Luzon. The color codes for the symbols represent different regions: west Luzon (in red), northwest Luzon (in gray), and Palawan (in black). Also shown here is the calculated paleo-relative sea level (shown as blue rectangles when IMCalc (Lorscheid and Rovere, 2019) is used and dashed lines if an average reef depth of 5 m is considered). Most of the dated corals are collected from the surfaces of the lowest terrace (TI). We observe that corals from Cape Bolinao and Pangasinan are relatively younger than the corals from northwest Luzon.

Table 4
Summary of sea-level indicators in west Luzon and Palawan Islands, Philippines and nomenclature used.

Cape Bolinao CRTs (this study)					Bolinao Reef Terraces (Maemoku and Paladio, 1992)		Currimao CRTs (Maxwell et al., 2018)			Palawan Notches		
Terrace level	Elevation (m)	Elevation uncertainty (m)	Coral ages (kyr)	Terrace width (km)	Elevation (m)	Terrace level	Elevation (m)	Coral ages (kyr)	Terrace level	Elevation (m)	Coral ages (kyr)	Indicator
TI[a]	3.87	± 0.01	6.382–5.71	< 10 m			3.4–3.7	7.373–6.163	TI	1.5 ± 0.15	6.7–5.69	LTN
TII[a]	5.72	± 0.02		< 20 m			6.1–6.6	6.774–6.533	TII			
TIII[a]	8.57	± 0.02		0.02–0.5	6.8–8.6	BVII	8.4–9.2		TIII			
TIV	31.42	± 13.75		0.1–1.0	21–23.1	BVI						
TV	55.15	± 14.66		0.5–1.8	30.2–59.2	BV						
TVI	80.55	± 12.52		0.1–0.3	43.6–74.7	BIV						
TVII	102.15	± 9.77		0.2–3	58.6–107.1	BIII						
TVIII	119.99	± 14.14		0.1–0.3	100–136	BII						
TIX	143.34	± 11.50		~5.0	120–155	BI	24–35	119.7–108.4	LPT	6.8 ± 0.15	126.5 ± 20	UTN

LPT: Late Pleistocene Terrace; LTN: Lower tidal notch (from Maeda et al. (2004)); UTN: Upper tidal notch (from Omura et al. (2004)).
[a] Measured elevation from discrete topographic survey transects.

uplift rate of 1.17 ± 0.03 mm/yr for Cape Bolinao and identify an east-southeast-directed tilt affecting the higher reef terraces, interpreted as MIS 5e based on reef stratigraphic simulations. This relatively high uplift rate, together with along-strike variations in CRT elevations and deformation patterns, provides compelling evidence for localized tectonic deformation. These observations are consistent with the influence of the Scarborough Seamount Chain subducting beneath Luzon Island, which likely plays a key role in shaping the forearc landscape. While our analysis is limited by lack of robust age constraints and glacial isostatic adjustment (GIA) corrections for the region, our study serves as the first attempt to provide a morpho-chronological framework for the development of late Quaternary CRTs in the northern Coral Triangle thereby presenting a key dataset especially in a region that is poorly studied. However, the knowledge on the vertical distribution of the carbonate sequences in Cape Bolinao (and other sites in the region) is still incomplete but required to fully constrain the reef response to relative sea-level changes. More importantly, future efforts should be done to constrain the timing of the older reef terraces by applying a broader suite of geochronological techniques, including strontium isotope stratigraphy, amino acid racemization, and cosmogenic nuclide dating, among others.

Supplementary data to this article can be found online at https://doi.org/10.1016/j.geomorph.2025.109796.

CRediT authorship contribution statement

Kathrine Maxwell: Writing – review & editing, Writing – original draft, Methodology, Investigation, Formal analysis, Data curation, Conceptualization. **Alessio Rovere:** Writing – review & editing, Supervision, Funding acquisition, Conceptualization. **Hildegard Westphal:** Writing – review & editing, Supervision, Resources, Funding acquisition, Conceptualization. **Kevin Garas:** Writing – review & editing, Investigation. **Mirasol Guinto:** Writing – review & editing, Investigation. **Denovan Chauveau:** Writing – review & editing, Formal analysis. **Hsun-Ming Hu:** Writing – review & editing, Formal analysis. **Chuan-Chou Shen:** Writing – review & editing, Resources, Funding acquisition, Formal analysis.

Funding sources

This research was supported by the program 4D-REEF, funded by the European Union's Horizon 2020 research and innovation program under the Marie Skłodowska-Curie Actions (grant no. 813360) to Hildegard Westphal. ^{230}Th dates using solution MC-ICPMS protocol for stalagmites were determined at the High-Precision Mass Spectrometry and Environment Change Laboratory (HISPEC), Department of Geosciences, National Taiwan University, supported by grants from Taiwan ROC MOST (111-2116-M-002-022-MY3 to Chuan-Chou Shen) and National Taiwan University (112L894202 to Chuan-Chou Shen).

Declaration of competing interest

The authors declare that they have no known competing financial interests or personal relationships that could have appeared to influence the work reported in this paper.

Acknowledgements

The authors acknowledge the doctoral program Marie Skłodowska-Curie Innovative Training Network (ITN) 4D-REEF, coordinated by Willem Renema. The authors also thank the following institutions: the Leibniz Centre for Tropical Marine Research (ZMT, Bremen) lab support; the National Mapping and Resource Information Authority (NAMRIA) for generously providing the 2013 airborne IFSAR-DTM topographic data; the Hydrography Branch of NAMRIA for their provision of actual tide gauge and bathymetric data; the Philippine Active Geodetic

Network (PAGeNet) - Geodesy Division/Mapping and Geodesy Branch of NAMRIA for granting access to real time corrections during RTK-GNSS surveys and for efficient technical support; and the Mines and Geosciences Bureau for their provision of necessary permits for the samples. The authors are grateful to the local government officials of the municipalities of Bolinao, Burgos, and Dasol and the province of Pangasinan for their support and permission to conduct field activities. We also thank Mari Shylla Joaquin for the logistical support and Sebastian Flotow for his valuable assistance with thin section preparation. We are grateful to Jody Webster and an anonymous reviewer for their insightful comments and suggestions, which significantly enhanced the clarity and quality of this manuscript. ^{230}Th dates using solution MC-ICPMS protocol for stalagmites were determined at the High-Precision Mass Spectrometry and Environment Change Laboratory (HISPEC), Department of Geosciences, National Taiwan University, supported by grants from Taiwan ROC MOST (111-2116-M-002-022-MY3 to C.-C.S.) and National Taiwan University (112L894202 to C.-C.S.). K.M. and H.W. were supported by funding from the European Union's Horizon 2020 research and innovation programme under the Marie Sklodowska-Curie Actions (Grant agreement No 813360). This publication is part of Kathrine Maxwell's doctoral thesis.

Data availability

Data will be made available on request.

References

Anthony, E.J., 2008. Chapter seven coral reef and carbonate shores. In: Anthony, E.J. (Ed.), Developments in Marine Geology, Shore Processes and Their Palaeoenvironmental Applications. Elsevier, pp. 325–367. https://doi.org/10.1016/S1572-5480(08)00407-7.

Armada, L.T., Hsu, S.-K., Dimalanta, C.B., Yumul Jr., G.P., Doo, W.-B., Yeh, Y.-C., 2020. Forearc structures and deformation along the Manila Trench. J. Asian Earth Sci. X 4, 100036. https://doi.org/10.1016/j.jaesx.2020.100036.

Armijo, R., Lacassin, R., Coudurier-Curveur, A., Carrizo, D., 2015. Coupled tectonic evolution of Andean orogeny and global climate. Earth Sci. Rev. 143, 1–35. https://doi.org/10.1016/j.earscirev.2015.01.005.

Bard, E., Jouannic, C., Hamelin, B., Pirazzoli, P., Arnold, M., Faure, G., Sumosusastro, P., Syaefudin, 1996. Pleistocene sea levels and tectonic uplift based on dating of corals from Sumba Island, Indonesia. Geophys. Res. Lett. 23, 1473–1476. https://doi.org/10.1029/96GL01279.

Bintanja, R., van de Wal, R.S.W., Oerlemans, J., 2005. Modelled atmospheric temperatures and global sea levels over the past million years. Nature 437, 125–128. https://doi.org/10.1038/nature03975.

Blanchon, P., Eisenhauer, A., 2001. Multi-stage reef development on Barbados during the Last Interglaciation. Quat. Sci. Rev. 20, 1093–1112. https://doi.org/10.1016/S0277-3791(00)00173-6.

Blanchon, P., Eisenhauer, A., Fietzke, J., Liebetrau, V., 2009. Rapid sea-level rise and reef back-stepping at the close of the last interglacial highstand. Nature 458, 881–884. https://doi.org/10.1038/nature07933.

Bloom, A.L., Broecker, W.S., Chappell, J.M.A., Matthews, R.K., Mesolella, K.J., 1974. Quaternary sea level fluctuations on a tectonic coast: new 230 Th/ 234 U dates from the Huon Peninsula, New Guinea. Quat. Res. 4, 185–205. https://doi.org/10.1016/0033-5894(74)90007-6.

Bosscher, H., Schlager, W., 1992. Computer simulation of reef growth. Sedimentology 39, 503–512. https://doi.org/10.1111/j.1365-3091.1992.tb02130.x.

Boyden, P., Stocchi, P., Rovere, A., 2023. Refining patterns of melt with forward stratigraphic models of stable Pleistocene coastlines. Earth Surf. Dyn. 11, 917–931. https://doi.org/10.5194/esurf-11-917-2023.

Broecker, W.S., Thurber, D.L., Goddard, J., Ku, T.-L., Mattews, R.K., Mesolella, K.J., 1968. Milankovitch hypothesis supported by precise dating of coral reefs and deep-sea sediments. Science 159, 297–300. https://doi.org/10.1126/science.159.3812.297.

Bronk Ramsey, C., 2009. Bayesian analysis of radiocarbon dates. Radiocarbon 51, 337–360. https://doi.org/10.2458/azu_js_rc.51.3494.

Bureau of Mines and Geosciences, 1985a. Geological Map of Bani Quadrangle.

Bureau of Mines and Geosciences, 1985b. Geological Map of Bolinao Quadrangle.

Camoin, G.F., Seard, C., Deschamps, P., Webster, J.M., Abbey, E., Braga, J.C., Iryu, Y., Durand, N., Bard, E., Hamelin, B., Yokoyama, Y., Thomas, A.L., Henderson, G.M., Dussouillez, P., 2012. Reef response to sea-level and environmental changes during the last deglaciation: Integrated Ocean Drilling Program Expedition 310, Tahiti Sea Level. Geology 40, 643–646. https://doi.org/10.1130/G32057.1.

Cantarero, D.L.M., Blanco, A., Cardenas, M.B., Nadaoka, K., Siringan, F.P., 2019. Offshore submarine groundwater discharge at a coral reef front controlled by faults. Geochem. Geophys. Geosyst. 20, 3170–3185. https://doi.org/10.1029/2019GC008310.

Chappell, J., 1974. Geology of coral terraces, Huon Peninsula, New Guinea: a study of quaternary tectonic movements and sea-level changes. GSA Bull. 85, 553–570. https://doi.org/10.1130/0016-7606(1974)85<553:GOCTHP>2.0.CO;2.

Chappell, J., Ota, Y., Berryman, K., 1996a. Late quaternary coseismic uplift history of Huon Peninsula, Papua New Guinea. Quat. Sci. Rev. 15, 7–22. https://doi.org/10.1016/0277-3791(95)00062-3.

Chappell, J., Omura, A., Esat, T., McCulloch, M., Pandolfi, J., Ota, Y., Pillans, B., 1996b. Reconciliation of late Quaternary sea levels derived from coral terraces at Huon Peninsula with deep sea oxygen isotope records. Earth Planet. Sci. Lett. 141, 227–236. https://doi.org/10.1016/0012-821X(96)00062-3.

Chauveau, D., Pastier, A., de Gelder, G., Husson, L., Authemayou, C., Pedoja, K., Cahyarini, S., 2023. Unravelling the morphogenesis of coastal terraces at Cape Laundi (Sumba Island, Indonesia): insights from numerical models. Earth Surf. Process. Landf. https://doi.org/10.1002/esp.5720.

Chauveau, D., Georgiou, N., Cerrone, C., Dean, S., Rovere, A., 2024. Sea-level oscillations within the last interglacial: insights from coral reef stratigraphic forward modelling. Quat. Sci. Rev. 336, 108759. https://doi.org/10.1016/j.quascirev.2024.108759.

Cheng, H., Lawrence Edwards, R., Shen, C.-C., Polyak, V.J., Asmerom, Y., Woodhead, J., Hellstrom, J., Wang, Y., Kong, X., Spötl, C., Wang, X., Calvin Alexander, E., 2013. Improvements in 230Th dating, 230Th and 234U half-life values, and U–Th isotopic measurements by multi-collector inductively coupled plasma mass spectrometry. Earth Planet. Sci. Lett. 371–372, 82–91. https://doi.org/10.1016/j.epsl.2013.04.006.

Chutcharavan, P.M., Dutton, A., Ellwood, M.J., 2018. Seawater 234U/238U recorded by modern and fossil corals. Geochim. Cosmochim. Acta 224, 1–17. https://doi.org/10.1016/j.gca.2017.12.017.

De Gelder, G., Jara-Muñoz, J., Melnick, D., Fernández-Blanco, D., Rouby, H., Pedoja, K., Husson, L., Armijo, R., Lacassin, R., 2020. How do sea-level curves influence modeled marine terrace sequences? Quat. Sci. Rev. 229, 106132. https://doi.org/10.1016/j.quascirev.2019.106132.

De Gelder, G., Husson, L., Pastier, A.-M., Fernández-Blanco, D., Pico, T., Chauveau, D., Authemayou, C., Pedoja, K., 2022. High interstadial sea levels over the past 420ka from the Huon Peninsula, Papua New Guinea. Commun. Earth Environ. 3, 1–12. https://doi.org/10.1038/s43247-022-00583-7.

De Gelder, G., Solihuddin, T., Utami, D.A., Hendrizan, M., Rachmayani, R., Chauveau, D., Authemayou, C., Husson, L., Cahyarini, S.Y., 2023. Geodynamic control on Pleistocene coral reef development: insights from northwest Sumba Island (Indonesia). Earth Surf. Process. Landf. 48, 2536–2553. https://doi.org/10.1002/esp.5643.

Deschamps, P., Durand, N., Bard, E., Hamelin, B., Camoin, G., Thomas, A.L., Henderson, G.M., Okuno, J., Yokoyama, Y., 2012. Ice-sheet collapse and sea-level rise at the Bølling warming 14,600 years ago. Nature 483, 559–564. https://doi.org/10.1038/nature10902.

Dominguez, S., Lallemand, S.E., Malavieille, J., von Huene, R., 1998. Upper plate deformation associated with seamount subduction. Tectonophysics 293, 207–224. https://doi.org/10.1016/S0040-1951(98)00086-9.

Dumitru, O.-A., Dyer, B., Austermann, J., Raymo, M., Goldstein, S., Creel, R., Sandstrom, M., Cashman, M., D'Andrea, W., Bolge, L., 2023. Last interglacial global mean sea level from high-precision U-series ages of Bahamian fossil coral reefs. Quat. Sci. Rev. 318. https://doi.org/10.1016/j.quascirev.2023.108287.

Dutton, A., Lambeck, K., 2012. Ice volume and sea level during the last interglacial. Science 337, 216–219. https://doi.org/10.1126/science.1205749.

Dyer, B., Austermann, J., D'Andrea, W.J., Creel, R.C., Sandstrom, M.R., Cashman, M., Rovere, A., Raymo, M.E., 2021. Sea-level trends across The Bahamas constrain peak last interglacial ice melt. Proc. Natl. Acad. Sci. 118, e2026839118. https://doi.org/10.1073/pnas.2026839118.

Dziewonski, A.M., Chou, T.-A., Woodhouse, J.H., 1981. Determination of earthquake source parameters from waveform data for studies of global and regional seismicity. J. Geophys. Res. Solid Earth 86, 2825–2852. https://doi.org/10.1029/JB086iB04p02825.

Ekström, G., Nettles, M., Dziewoński, A.M., 2012. The global CMT project 2004–2010: centroid-moment tensors for 13,017 earthquakes. Phys. Earth Planet. Inter. 200–201, 1–9. https://doi.org/10.1016/j.pepi.2012.04.002.

Fernández-Blanco, D., de Gelder, G., Lacassin, R., Armijo, R., 2020. Geometry of flexural uplift by continental rifting in Corinth, Greece. Tectonics 39, e2019TC005685. https://doi.org/10.1029/2019TC005685.

Flores, P.C.M., Siringan, F.P., Mateo, Z.R.P., Marfito, B.J., Sarmiento, K.J.S., Abigania, M. I.T., Daag, A.S., Maac-Aguilar, Y., 2023. Shallow structures, interactions, and recurrent vertical motions of active faults in Lingayen Gulf, Philippines. J. Asian Earth Sci. X 9, 100152. https://doi.org/10.1016/j.jaesx.2023.100152.

Gatchalian, R.C., Forsberg, R., Olesen, A.V., 2021. A new Philippine geoid model from airborne and terrestrial gravity data. Terr. Atmos. Ocean. Sci. 32, 913–920. https://doi.org/10.3319/TAO.2021.11.15.01.

GEBCO Compilation Group, 2023. GEBCO 2023 Grid. https://doi.org/10.5285/f98b053b-0cbc-6c23-e053-6c86abc0af7b.

Gervasio, F.C., 1967. Age and nature of orogenesis of the Philippines. Tectonophysics 4, 379–402. https://doi.org/10.1016/0040-1951(67)90006-6.

Grant, K.M., Rohling, E.J., Ramsey, C.B., Cheng, H., Edwards, R.L., Florindo, F., Heslop, D., Marra, F., Roberts, A.P., Tamisiea, M.E., Williams, F., 2014. Sea-level variability over five glacial cycles. Nat. Commun. 5, 5076. https://doi.org/10.1038/ncomms6076.

Hayes, D.E., Lewis, S.D., 1985. Structure and tectonics of the Manila trench system, Western Luzon, Philippines. Energy 10, 263–279. https://doi.org/10.1016/0360-5442(85)90046-5.

Heaton, T.J., Köhler, P., Butzin, M., Bard, E., Reimer, R.W., Austin, W.E.N., Ramsey, C.B., Grootes, P.M., Hughen, K.A., Kromer, B., Reimer, P.J., Adkins, J., Burke, A., Cook, M.

S., Olsen, J., Skinner, L.C., 2020. Marine20—the marine radiocarbon age calibration curve (0–55,000 cal BP). Radiocarbon 62, 779–820. https://doi.org/10.1017/RDC.2020.68.
Henry, H., Regard, V., Pedoja, K., Husson, L., Martinod, J., Witt, C., Heuret, A., 2014. Upper Pleistocene uplifted shorelines as tracers of (local rather than global) subduction dynamics. J. Geodyn. 78, 8–20. https://doi.org/10.1016/j.jog.2014.04.001.
Hiess, J., Condon, D.J., McLean, N., Noble, S.R., 2012. 238U/235U systematics in terrestrial uranium-bearing minerals. Science 335, 1610–1614. https://doi.org/10.1126/science.1215507.
Hoeksema, B., 2007. Delineation of the Indo-Malayan centre of maximum marine biodiversity: the Coral Triangle. In: Topics Geobiol, pp. 117–178. https://doi.org/10.1007/978-1-4020-6374-9_5.
Hsu, Y.-J., Yu, S.-B., Song, T.-R.A., Bacolcol, T., 2012. Plate coupling along the Manila subduction zone between Taiwan and northern Luzon. J. Asian Earth Sci. 51, 98–108. https://doi.org/10.1016/j.jseaes.2012.01.005.
Husson, L., Pastier, A.-M., Pedoja, K., Elliot, M., Paillard, D., Authemayou, C., Sarr, A.-C., Schmitt, A., Cahyarini, S.Y., 2018. Reef carbonate productivity during quaternary sea level oscillations. Geochem. Geophys. Geosyst. 19, 1148–1164. https://doi.org/10.1002/2017GC007335.
Inagaki, M., Omura, A., 2006. Uranium-series age of the highest marine terrace of the upper pleistocene on Kikai Island, Central Ryukyus, Japan. Quat. Res. (Daiyonki-Kenkyu) 45, 41–48. https://doi.org/10.4116/jaqua.45.41.
Jaffey, A.H., Flynn, K.F., Glendenin, L.E., Bentley, W.C., Essling, A.M., 1971. Precision measurement of half-lives and specific activities of 235U and 238U. Phys. Rev. C 4, 1889–1906. https://doi.org/10.1103/PhysRevC.4.1889.
Janssen, A.W., 2007. Holoplanktonic Mollusca (Gastropoda: Pterotracheoidea, Janthinoidea, Thecosomata and Gymnosomata) From the Pliocene of Pangasinan (Luzon, Philippines).
Jara-Muñoz, J., Melnick, D., Strecker, M.R., 2016. TerraceM: a MATLAB® tool to analyze marine and lacustrine terraces using high-resolution topography. Geosphere 12, 176–195. https://doi.org/10.1130/GES01208.1.
Jara-Muñoz, J., Melnick, D., Pedoja, K., Strecker, M.R., 2019. TerraceM-2: a Matlab® interface for mapping and modeling marine and lacustrine terraces. Front. Earth Sci. 7. https://doi.org/10.3389/feart.2019.00255.
Koelling, M., Webster, J.M., Camoin, G., Iryu, Y., Bard, E., Seard, C., 2009. SEALEX — internal reef chronology and virtual drill logs from a spreadsheet-based reef growth model. In: Global and Planetary Change, Quaternary Sea-level Changes : Records and Processes, 66, pp. 149–159. https://doi.org/10.1016/j.gloplacha.2008.07.011.
Lajoie, K.R., 1986. Coastal tectonics. In: Wallace, R. (Ed.), Active Tectonics: Impact on Society. National Academic Press, Washington, DC, pp. 95–124.
Lambeck, K., Chappell, J., 2001. Sea level change through the last glacial cycle. Science 292, 679–686. https://doi.org/10.1126/science.1059549.
Lorscheid, T., Rovere, A., 2019. The indicative meaning calculator – quantification of paleo sea-level relationships by using global wave and tide datasets. Open Geospat. Data Softw. Stand. 4, 10. https://doi.org/10.1186/s40965-019-0069-8.
Maeda, Y., Siringan, F., Omura, A., Berdin, R., Hosono, Y., Atsumi, S., Nakamura, T., 2004. Higher-than-present Holocene mean sea levels in Ilocos, Palawan and Samar, Philippines. Quat. Int. 115–116, 15–26. https://doi.org/10.1016/S1040-6182(03)00093-4.
Maemoku, H., Paladio, J., 1992. Raised Coral Reefs at Bolinao, northwestern Luzon Island of the Philippines. Geogr. Sci. 47, 183–189.
Maxwell, K., 2024. Late Quaternary Relative Sea-level Changes and Reef Development in the Coral Triangle Recorded by Coral Reef Terraces. https://doi.org/10.26092/elib/3409.
Maxwell, K., Westphal, H., Rovere, A., 2021. A standardized database of Last Interglacial (MIS 5e) sea-level indicators in Southeast Asia. Earth Syst. Sci. Data 13, 4313–4329. https://doi.org/10.5194/essd-13-4313-2021.
Maxwell, K.V., Ramos, N.T., Tsutsumi, H., Chou, Y.-C., Duan, F., Shen, C.-C., 2018. Late Quaternary uplift across northwest Luzon Island, Philippines constrained from emergent coral reef terraces. Earth Surf. Process. Landf. 43, 3114–3132. https://doi.org/10.1002/esp.4474.
McGregor, H.V., Abram, N.J., 2008. Images of diagenetic textures in Porites corals from Papua New Guinea and Indonesia: images of coral diagenetic textures. Geochem. Geophys. Geosyst. 9. https://doi.org/10.1029/2008GC002093 n/a-n/a.
McManus, J.W., Nañola Jr., C.L., Reyes Jr., R.B., Kesner, K.N., 1992. Resource Ecology of the Bolinao Coral Reef System. International Center for Living Aquatic Resources Management Stud. Rev. 22, Manila.
Mesolella, K.J., 1967. Zonation of Uplifted Pleistocene Coral Reefs on Barbados, West Indies. Sci. New Ser. 156, 638–640.
Mines and Geosciences Bureau, 2010. Geology of the Philippines. In: Geology of the Philippines. Department of Environment and Natural Resources, North Avenue, Quezon City, Philippines.
Omura, A., Maeda, Y., Kawana, T., Siringan, F.P., Berdin, R.D., 2004. U-series dates of Pleistocene corals and their implications to the paleo-sea levels and the vertical displacement in the Central Philippines. Quat. Int. 115–116, 3–13. https://doi.org/10.1016/S1040-6182(03)00092-2.
Ota, Y., Omura, A., 1992. Contrasting styles and rates of tectonic uplift of coral reef terraces in the Ryukyu and Daito Islands, southwestern Japan. Quat. Int. 15–16, 17–29. https://doi.org/10.1016/1040-6182(92)90033-X.
Pastier, A.-M., Husson, L., Pedoja, K., Bézos, A., Authemayou, C., Arias-Ruiz, C., Cahyarini, S.Y., 2019. Genesis and architecture of sequences of quaternary coral reef terraces: insights from numerical models. Geochem. Geophys. Geosyst. 20, 4248–4272. https://doi.org/10.1029/2019GC008239.
Pautot, G., Rangin, C., 1989. Subduction of the South China Sea axial ridge below Luzon (Philippines). Earth Planet. Sci. Lett. 92, 57–69. https://doi.org/10.1016/0012-821X(89)90020-4.
Pedoja, K., Husson, L., Regard, V., Cobbold, P.R., Ostanciaux, E., Johnson, M.E., Kershaw, S., Saillard, M., Martinod, J., Furgerot, L., Weill, P., Delcaillau, B., 2011. Relative sea-level fall since the last interglacial stage: are coasts uplifting worldwide? Earth Sci. Rev. 108, 1–15. https://doi.org/10.1016/j.earscirev.2011.05.002.
Pedoja, K., Husson, L., Bezos, A., Pastier, A.-M., Imran, A.M., Arias-Ruiz, C., Sarr, A.-C., Elliot, M., Pons-Branchu, E., Nexer, M., Regard, V., Hafidz, A., Robert, X., Benoit, L., Delcaillau, B., Authemayou, C., Dumoulin, C., Choblet, G., 2018. On the long-lasting sequences of coral reef terraces from SE Sulawesi (Indonesia): distribution, formation, and global significance. Quat. Sci. Rev. 188, 37–57. https://doi.org/10.1016/j.quascirev.2018.03.033.
Peñalver, L., Pedoja, K., Martin-Izquierdo, D., Authemayou, C., Nuñez, A., Chauveau, D., de Gelder, G., Davilan, P., Husson, L., 2021. The Cuban staircase sequences of coral reef and marine terraces: a forgotten masterpiece of the Caribbean geodynamical puzzle. Mar. Geol. 440, 106575. https://doi.org/10.1016/j.margeo.2021.106575.
Philippine Institute of Volcanology and Seismology (PHIVOLCS), 2020. Distribution of Active Faults and Trenches (Map).
Pirazzoli, P.A., Radtke, U., Hantoro, W.S., Jouannic, C., Hoang, C.T., Causse, C., Best, M. B., 1991. Quaternary Raised Coral-Reef Terraces on Sumba Island, Indonesia. Science 252, 1834–1836. https://doi.org/10.1126/science.252.5014.1834.
Pirazzoli, P.A., Radtke, U., Hantoro, W.S., Jouannic, C., Hoang, C.T., Causse, C., Best, M. B., 1993. A one million-year-long sequence of marine terraces on Sumba Island, Indonesia. Mar. Geol. 109, 221–236. https://doi.org/10.1016/0025-3227(93)90062-Z.
Quimpo, T.J.R., Requilme, J.N.C., Gomez, E.J., Sayco, S.L.G., Tolentino, M.P.S., Cabaitan, P.C., 2020. Low coral bleaching prevalence at the Bolinao-Anda Reef Complex, northwestern Philippines during the 2016 thermal stress event. Mar. Pollut. Bull. 160, 111567. https://doi.org/10.1016/j.marpolbul.2020.111567.
Ramos, N.T., Tsutsumi, H., 2010. Evidence of large prehistoric offshore earthquakes deduced from uplifted Holocene marine terraces in Pangasinan Province, Luzon Island, Philippines. Tectonophysics 495, 145–158. https://doi.org/10.1016/j.tecto.2010.08.007.
Rangin, C., Le Pichon, X., Mazzotti, S., Pubellier, M., Chamot-Rooke, N., Aurelio, M., Walpersdorf, A., Quebral, R., 1999. Plate convergence measured by GPS across the Sundaland/Philippine Sea Plate deformed boundary: the Philippines and eastern Indonesia. Geophys. J. Int. 139, 296–316. https://doi.org/10.1046/j.1365-246x.1999.00969.x.
Reimer, R.W., Reimer, P.J., 2017. An online application for ΔR calculation. Radiocarbon 59, 1623–1627. https://doi.org/10.1017/RDC.2016.117.
Rohling, E.J., Grant, K., Bolshaw, M., Roberts, A.P., Siddall, M., Hemleben, C., Kucera, M., 2009. Antarctic temperature and global sea level closely coupled over the past five glacial cycles. Nat. Geosci. 2, 500–504. https://doi.org/10.1038/ngeo557.
Rovere, A., Raymo, M.E., Vacchi, M., Lorscheid, T., Stocchi, P., Gómez-Pujol, L., Harris, D.L., Casella, E., O'Leary, M.J., Hearty, P.J., 2016. The analysis of Last Interglacial (MIS 5e) relative sea-level indicators: reconstructing sea-level in a warmer world. Earth Sci. Rev. 159, 404–427. https://doi.org/10.1016/j.earscirev.2016.06.006.
Schellmann, G., Radtke, U., 2004. A revised morpho- and chronostratigraphy of the Late and Middle Pleistocene coral reef terraces on Southern Barbados (West Indies). Earth Sci. Rev. 64, 157–187. https://doi.org/10.1016/S0012-8252(03)00043-6.
Schwanghart, W., Scherler, D., 2014. Short communication: TopoToolbox 2 – MATLAB-based software for topographic analysis and modeling in Earth surface sciences. Earth Surf. Dyn. 2, 1–7. https://doi.org/10.5194/esurf-2-1-2014.
Shaish, L., Levy, G., Katzir, G., Rinkevich, B., 2010. Coral reef restoration (Bolinao, Philippines) in the face of frequent natural catastrophes. Restor. Ecol. 18, 285–299. https://doi.org/10.1111/j.1526-100X.2009.00647.x.
Shen, C.-C., Cheng, H., Edwards, R.L., Moran, S.B., Edmonds, H.N., Hoff, J.A., Thomas, R. B., 2003. Measurement of attogram quantities of 231Pa in dissolved and particulate fractions of seawater by isotope dilution thermal ionization mass spectroscopy. Anal. Chem. 75, 1075–1079. https://doi.org/10.1021/ac026247r.
Shen, C.-C., Li, K.-S., Sieh, K., Natawidjaja, D., Cheng, H., Wang, X., Edwards, R.L., Lam, D.D., Hsieh, Y.-T., Fan, T.-Y., Meltzner, A.J., Taylor, F.W., Quinn, T.M., Chiang, H.-W., Kilbourne, K.H., 2008. Variation of initial 230Th/232Th and limits of high precision U–Th dating of shallow-water corals. Geochim. Cosmochim. Acta 72, 4201–4223. https://doi.org/10.1016/j.gca.2008.06.011.
Shen, C.-C., Siringan, F.P., Lin, K., Dai, C.-F., Gong, S.-Y., 2010. Sea-level rise and coral-reef development of Northwestern Luzon since 9.9ka. Palaeogeogr. Palaeoclimatol. Palaeoecol. 292, 465–473. https://doi.org/10.1016/j.palaeo.2010.04.007.
Shen, C.-C., Lin, K., Duan, W., Jiang, X., Partin, J.W., Edwards, R.L., Cheng, H., Tan, M., 2013. Testing the annual nature of speleothem banding. Sci. Rep. 3, 2633. https://doi.org/10.1038/srep02633.
Spratt, R.M., Lisiecki, L.E., 2016. A Late Pleistocene sea level stack. Clim. Past 12, 1079–1092. https://doi.org/10.5194/cp-12-1079-2016.
Torres, A.F., Valino, D.A.M., Ravago-Gotanco, R., 2021. Zooxanthellae diversity and coral-symbiont associations in the Philippine Archipelago: specificity and adaptability across thermal gradients. Front. Mar. Sci. 8.
Vergara, M.W.B., Geronimo, R.C., Ticzon, V.S., Dizon, R.M., Villanueva, V.S., Baria, M. V., Vicentuan-Cabaitan, K.D., Dela Cruz, D.W., Bollozos, I.S., Ravago-Gotangco, R., 2010. Status of coral reef research in Bolinao-Anda reef complex, northwestern Philippines. In: Building Capacity in Coral Reef Science: An Anthology of CRTR Scholars' Research 2010. Coral Reef Targeted Research & Capacity Building for Management (CRTR) Program.

Veron, J., Stafford-Smith, M., DeVantier, L., Turak, E., 2015. Overview of distribution patterns of zooxanthellate Scleractinia. Front. Mar. Sci. 1. https://doi.org/10.3389/fmars.2014.00081.

Veron, J.E.N., Devantier, L.M., Turak, E., Green, A.L., Kininmonth, S., Stafford-Smith, M., Peterson, N., 2009. Delineating the Coral Triangle. Galaxea J. Coral Reef Stud. 11, 91–100. https://doi.org/10.3755/galaxea.11.91.

Waelbroeck, C., Labeyrie, L., Michel, E., Duplessy, J.C., McManus, J.F., Lambeck, K., Balbon, E., Labracherie, M., 2002. Sea-level and deep water temperature changes derived from benthic foraminifera isotopic records. Quat. Sci. Rev. 21, 295–305. https://doi.org/10.1016/S0277-3791(01)00101-9.

Wang, K., Bilek, S.L., 2011. Do subducting seamounts generate or stop large earthquakes? Geology 39, 819–822. https://doi.org/10.1130/G31856.1.

Wani, R., Ocampo, R., Aguilar, Y., Zepeda, M., Kurihara, Y., Hagino, K., Hayashi, H., Kase, T., 2008. First discovery of fossil Nautilus pompilius Linnaeus, 1758 (Nautilidae, Cephalopoda) from Pangasinan, northwestern Philippines. Paleontol. Res. 12, 89–95. https://doi.org/10.2517/1342-8144(2008)12[89:FDOFNP]2.0.CO;2.

Wessel, P., Luis, J.F., Uieda, L., Scharroo, R., Wobbe, F., Smith, W.H.F., Tian, D., 2019. The Generic Mapping Tools Version 6. Geochem. Geophys. Geosyst. 20, 5556–5564. https://doi.org/10.1029/2019GC008515.

Woodroffe, C.D., Webster, J.M., 2023. Coral records of relative sea-level changes. In: Reference Module in Earth Systems and Environmental Sciences. Elsevier. https://doi.org/10.1016/B978-0-323-99931-1.00052-0 p. B9780323999311000520.

Yokoyama, Y., Esat, T., 2011. Global climate and sea level: enduring variability and rapid fluctuations over the past 150,000 years. Oceanography 24, 54–69. https://doi.org/10.5670/oceanog.2011.27.